Binary Asteroid Population. 2. Anisotropic distribution of orbit poles

P. Pravec [a], P. Scheirich [a], D. Vokrouhlický [b], A. W. Harris [c], P. Kušnirák [a], K. Hornoch [a], D. P. Pray [d], D. Higgins [e], A. Galád [a,f], J. Világi [f], Š. Gajdoš [f], L. Kornoš [f], J. Oey [g], M. Husárik [h], W. R. Cooney [i], J. Gross [i], D. Terrell [i,j], R. Durkee [k], J. Pollock [ℓ], D. Reichart [m], K. Ivarsen [m], J. Haislip [m], A. LaCluyze [m], Yu. N. Krugly [n], N. Gaftonyuk [o], R. D. Stephens [p], R. Dyvig [q], V. Reddy [r], V. Chiorny [n], O. Vaduvescu [s,t], P. Longa-Peña [s,u], A. Tudorica [v,w], B. D. Warner [x], G. Masi [y], J. Brinsfield [z], R. Gonçalves [aa], P. Brown [ab], Z. Krzeminski [ab], O. Gerashchenko [ac], V. Shevchenko [n], I. Molotov [ad], F. Marchis [ae,af]

[a] *Astronomical Institute, Academy of Sciences of the Czech Republic, Fričova 1, CZ-25165 Ondřejov, Czech Republic*

[b] *Institute of Astronomy, Charles University, Prague, V Holešovičkách 2, CZ-18000 Prague 8, Czech Republic*

[c] *4603 Orange Knoll Avenue, La Cañada, CA 91011, U.S.A.*

[d] *Carbuncle Hill Observatory, W. Brookfield, MA, U.S.A.*

[e] *Hunters Hill Observatory, Ngunnawal, Canberra, Australia*

[f] *Modra Observatory, Department of Astronomy, Physics of the Earth, and Meteorology, FMFI UK, Bratislava SK-84248, Slovakia*

[g] *Leura Observatory, Leura, N.S.W., Australia*

[h] *Astronomical Institute of the Slovak Academy of Sciences, SK-05960 Tatranská Lomnica, Slovakia*

[i] *Sonoita Research Observatory, 77 Paint Trail, Sonoita, AZ 85637, U.S.A.*

[j] *Deptartment of Space Studies, Southwest Research Institute, Boulder, CO 80302, U.S.A.*

[k] *Shed of Science Observatory, 5213 Washburn Ave. S, Minneapolis, MN 55410, U.S.A.*

[ℓ] *Physics and Astronomy Department, Appalachian State University, Boone, NC 28608, U.S.A.*

[m] *Physics and Astronomy Department, University of North Carolina, Chapel Hill, NC 27514, U.S.A.*

[n] *Institute of Astronomy of Kharkiv National University, Sumska Str. 35, Kharkiv 61022, Ukraine*

[o] *Crimean Astrophysical Observatory, Simeiz Department, Simeiz 98680, Crimea, Ukraine*

[p] *Center for Solar System Studies, 8300 Utica Avenue, Suite 105, Rancho Cucamonga, CA 91730, U.S.A.*

[q] *Badlands Observatory, 12 Ash Street, P.O. Box 37, Quinn, SD 57775, U.S.A.*

[r] *Department of Space Studies, University of North Dakota, Grand Forks, U.S.A.*

[s] *Instituto de Astronomia, Universidad Catolica del Norte, Avenida Angamos 0610, Antofagasta, Chile*

[t] *Isaac Newton Group of Telescopes, La Palma, Apartado de correos 321, E-38700 Santa Cruz de la Palma, Canary Islands, Spain*

[u] *University of Warwick, Department of Physics, Coventry CV4 7AL, U.K.*

[v] *University of Bucharest, Faculty of Physics, Str. Fizicienilor nr. 1, CP Mg – 11, Bucharest-Magurele 76900, Romania*

[w] *Argelander Institute for Astronomy – Bonn University, Auf dem Huegel 71 D-53121, Germany*

[x] *Palmer Divide Observatory, 17995 Bakers Farm Rd., Colorado Springs, CO 80908, U.S.A.*

[y] *Campo Catino Observatory, I-03016 Guarcino, Italy*

[z] *Via Capote Observatory, Thousand Oaks, CA, U.S.A.*

[aa] *Obs. Ast. de Linhaceira, Escola Superior de Tecnologia de Tomar, Instituto Politecnico de Tomar, 2300-313 Tomar, Portugal*

[ab] *Elginfield Observatory, Department of Physics & Astronomy, University of Western Ontario, London, Ontario N6A 3K7, Canada*

[ac] *Andrushivka Astronomical Observatory, Ukraine*

[ad] *Keldysh Institute of Applied Mathematics, Russian Academy of Sciences, Miusskaya sq. 4, Moscow 125047, Russia*

[ae] *Carl Sagan Center at the SETI Institute, 189 Bernado Av., Mountain View, CA 94043, U.S.A.*

[af] *Department of Astronomy, University of California at Berkeley, Berkeley, CA 94720, U.S.A.*

2011 July 26, submitted to Icarus

Editorial correspondence to:
Dr. Petr Pravec
Astronomical Institute AS CR
Fričova 1
Ondřejov
CZ-25165
Czech Republic
Phone: 00420-323-620352
Fax: 00420-323-620263
E-mail address: ppravec@asu.cas.cz

Abstract

Our photometric observations of 18 main-belt binary systems in more than one apparition revealed a strikingly high number of 15 having positively re-observed mutual events in the return apparitions. Our simulations of the survey showed that it cannot be due to an observational selection effect and that the data strongly suggest that poles of mutual orbits between components of binary asteroids in the primary size range 3–8 km are not distributed randomly: The null hypothesis of an isotropic distribution of the orbit poles is rejected at a confidence level greater than 99.99%. Binary orbit poles concentrate at high ecliptic latitudes, within 30° of the poles of the ecliptic. We propose that the binary orbit poles oriented preferentially up/down-right are due to either of the two processes: (i) the YORP tilt of spin axes of their parent bodies toward the asymptotic states near obliquities 0 and 180° (pre-formation mechanism), or (ii) the YORP tilt of spin axes of the primary components of already formed binary systems toward the asymptotic states near obliquities 0 and 180° (post-formation mechanism). The alternative process of elimination of binaries with poles closer to the ecliptic by the Kozai dynamics of gravitational perturbations from the sun does not explain the observed orbit pole concentration as in the close asteroid binary systems the J_2 perturbation due to the primary dominates the solar-tide effect.

Key words: Asteroids, binary;

1 Introduction

An orientation of the orbit of components of a binary asteroid around their common center of mass can be estimated from photometric observations of their mutual events — occultations/eclipses. It requires observations taken over a range of geometries of the system with respect to Earth and Sun. Scheirich and Pravec (2009) derived or constrained orbit poles of 5 near-Earth asteroid binaries, taking advantage of rapid changes of viewing geometries of the near-Earth binaries during their approaches to Earth. Binary systems in the main belt of asteroids show a limited change of observing geometry during one apparition [1] and observations over 2–3 apparitions are typically needed to estimate the orientation (ecliptic longitude and latitude of the pole) of the mutual orbit for a main-belt asteroid (MBA) binary.

We observed 18 MBA binaries in 2–3 apparitions. With our modeling technique that we used for the five NEA binaries two years ago, we estimated or constrained their mutual orbits (see Sect. 5). An interpretation of the sample of derived binary parameters must take into account existing observational biases, see a theory of the selection effects of the photometric technique of binary detection presented in Sect. 2. A direct estimation of the biases present in the discovered sample of binaries is complicated by a limited probability of covering the mutual event in a binary with *a priori* unknown orbit period with a given set of survey observations. This complication is overcome with analysis of the statistics of re-detections of mutual events in the binaries in their return apparitions. The key advantage is that a time distribution of the planned follow-up observations of the binaries in the return apparitions was matched to the orbit periods determined in the discovery apparition, which made our simulations of the observational selection effects feasible and easy.

2 Probability of photometric detection of a binary asteroid

The probability of the photometric detection of a binary asteroid is formulated as follows:

$$P_{\rm det} = p_{\rm me}\, p_{\rm cov}\, p_{\rm res}, \tag{1}$$

where $p_{\rm me}$ is a probability of occurence of a mutual event (occultation or eclipse) between the components of the system, $p_{\rm cov}$ is a probability of covering the mutual event with a given set of observations, and $p_{\rm res}$ is a probability of resolving the mutual event with the given photometric observations.

[1] An asteroid's photometric apparition is a time interval, usually a few weeks to a few months long, when the asteroid is in favorable conditions (brightness, solar elongation) allowing photometric observations of required accuracy and duration during night. For main belt asteroids, it occurs around opposition with the Sun.

The probability of occurence of a mutual event depends on the parameters of the system:

$$p_{\rm me} \equiv p_{\rm me}(\epsilon, a_{\rm orb}, e, D_1, D_2, \text{component shapes}, \text{phase effect}), \tag{2}$$

where ϵ is an obliquity of the mutual orbit of the binary components, $a_{\rm orb}$ and e are its semimajor axis and eccentricity, D_i is a mean diameter of the i-th component ($D_2 \leq D_1$), and the probability also depends on shapes of the components and their phase effect. While a dependence of the probability on the component shapes and phase effect is complex and can be described with a numerical model, it is illustrative to use the following analytical formula for a case of spherical components, zero eccentricity of the mutual orbit, and zero solar phase:

$$p_{\rm me} = \begin{cases} 1, & \text{if } \epsilon \leq i_{\rm c} \text{ or } \epsilon \geq (\pi - i_{\rm c}), \\ \frac{2}{\pi} \arcsin \frac{\sin i_{\rm c}}{\sin \epsilon}, & \text{if } i_{\rm c} < \epsilon < (\pi - i_{\rm c}), \end{cases} \tag{3}$$

where

$$i_{\rm c} = \arcsin \frac{1 + \frac{D_2}{D_1}}{2\frac{a_{\rm orb}}{D_1}}. \tag{4}$$

The mean probability of occurence of mutual events is

$$P_{\rm me} = \frac{\int_0^\pi p_{\rm me}(\epsilon) f(\epsilon)\, {\rm d}\epsilon}{\int_0^\pi f(\epsilon)\, {\rm d}\epsilon}, \tag{5}$$

where $f(\epsilon)$ is a number density of binary orbit poles. In the case of the isotropic distribution of binary orbits, $f(\epsilon) = \sin \epsilon$, we get

$$P_{\rm me} = 1 - \cos i_{\rm c} + \int_{i_{\rm c}}^{\pi/2} p_{\rm me}(\epsilon) \sin \epsilon\, {\rm d}\epsilon. \tag{6}$$

These formulas show that the probability of occurence of mutual events reaches a minimum at obliquity $\epsilon = \pi/2$ and that the mean probability decreases with increasing relative distance $a_{\rm orb}/D_1$ between the components. This describes an existing observational selection effect favoring detections of close systems and those with mutual orbit poles oriented up/down-right.

The probability of covering the mutual event with a given set of observations:

$$p_{\rm cov} \equiv p_{\rm cov}(P_{\rm orb}, \text{time distribution of observations}), \tag{7}$$

where $P_{\rm orb}$ is a period of the mutual orbit of the binary components. For a given distribution of observations, the probability has to be computed with

a numerical model. Nevertheless, a general trend is that this probability decreases with increasing orbit period, further strengthening the selection effect towards close systems. This probability is usually less than 1 for observations of a previously unknown binary where the orbit period is not known *a priori* and thus a distribution of the observations cannot be matched to the orbit period. In a case of planned re-observations of a known binary with determined orbit period, however, the probability can be effectively set to 1 with scheduling the observations so that to cover the full orbit. This highly simplifies simulations of planned observations of known binaries in their return apparitions and allows us to constrain a distribution of their orbit poles with analysis of the re-observations in the post-discovery apparitions.

The probability of resolving mutual event, $p_{\rm res}$, depends on a depth of the mutual event (F) and photometric quality of the observations. The depth of (relative brightness attenuation in) a total secondary event at zero solar phase is $F_{\rm sec} = I_2/(I_1 + I_2)$, where I_i is a light flux from the i-th component. For components with the same albedo observed at zero phase angle, it converts to $F_{\rm sec} = [1 + (D_1/D_2)^2]^{-1}$, and the depth of the primary event is $F_{\rm prim} = F_{\rm sec}$. At non-zero phase angles and for non-central events, the depth of the mutual event is computed with a numerical model, assuming a specific scattering law. The photometric quality of the observations affects the probability of resolving the mutual event substantially. Generally, events with depth much greater than photometric errors of the observations are resolved with a probability approaching 1, while events with depth lower than the photometric errors are usually burried in the noise and the probability of resolving them is close to 0. For observations producing controlled and homogeneous data, the probability of resolving mutual event is approximated with a step function:

$$p_{\rm res} = \begin{cases} 0, & \text{if } F < F_{\rm lim}, \\ 1, & \text{if } F \geq F_{\rm lim}, \end{cases} \tag{8}$$

where $F_{\rm lim}$ is a minimum detectable relative brightness attenuation.

Being equipped with the theory of photometric detection of a binary asteroid, we will intrepret our observations of binary asteroids presented in Section 3 with simulations of the survey observations given in Section 4.

3 Observations

We run a long-term project of photometric observations of binary systems among small asteroids called "Photometric Survey for Asynchronous Binary Asteroids" since 2005. The collaborating station Palmer Divide Observatory runs a parallel survey project aimed at describing rotations and binary systems in the Hungaria asteroids group (Warner et al. 2009a,b). Both surveys used similar observing techniques and strategies, and they actually cooperated

and coordinated their observations; there was a major overlap of the lists of stations participating in the two surveys. We joined observations of binaries made within the two cooperating surveys and analysed them together as they effectively worked as one joint binary asteroids survey.

Of 45 MBA binaries that we detected within the surveys by May 2011, we re-observed 18 of them in their return apparitions. Their list and selected parameters are given in Table 1. The listed parameters are following: the mean diameter of the primary at the equatorial aspect (D_1), the ratio between the mean diameters of the components of the binary (D_2/D_1), the rotation period of the primary (P_1), the orbit period ($P_{\rm orb}$), the rotation period of the secondary (P_2), the relative size of the mutual orbit's semi-major axis ($a_{\rm orb}/D_1$), ranges of admissible values of the mutual orbit pole's ecliptic longitude, latitude, and obliquity to the current heliocentric orbit ($L_{\rm p}$, $B_{\rm p}$, ϵ), the semi-major axis ($a_{\rm h}$) and inclination ($i_{\rm h}$) of the system's heliocentric orbit (epoch 2011 Aug. 27.0 TT). These parameters were estimated from our observations using methods described in Pravec et al. (2006), Pravec and Harris (2007), and Scheirich and Pravec (2009). The results for 9 systems for which we got a unique orbit solution are presented in Section 5; their observations as well as additional results are given in the electronic Supplementary Information. The table with the estimated parameters, including their uncertainties and references, is available on web page http://www.asu.cas.cz/∼asteroid/binastdata.htm. The original photometric data will be stored in ALCDEF archive (Stephens et al. 2010).

Of the 18 binaries observed in more than one apparition, we detected mutual events in 15 also upon their return. In the three cases of negative event detection in the return apparition, there were observed no apparent attenuations with relative depth of 4% or greater. We cannot rule out possible occurence of very shallow events with depths below the 4%-event depth detection limit of our survey, due to grazing eclipses or occultations; an occurence of such near-boundary events producing attenuations below the detection limit are accounted for in the model of the survey that we present in the next section.

In Table 2, we list epochs and asteroid's ecliptic longitudes and latitudes with respect to Earth (L, B) and Sun ($L_{\rm h}, B_{\rm h}$) of the first positive event detection in both the discovery and the return apparitions for each of the 18 binaries. For the three systems that did not show mutual events in the return apparition, we list an epoch of the observing session closest to the middle of the observational run (that lasted from 3 to 17 days in the three cases).

The rate of positive re-detections is strikingly high. We simulated the survey, tested the null hypothesis of anisotropic distribution of binary orbit poles and found that it is rejected at a high confidence level. We found that poles of mutual orbits of small binaries concentrate at high ecliptic latitudes around the poles of the ecliptic. We present the simulations and findings in the following section.

4 Simulations of the survey

We constructed a numerical model of the survey to simulate the observed re-detections of mutual events in the 18 binaries observed in more than one apparition. The model is analogous to that we used for simulations of our survey for near-Earth asteroids in Pravec et al. (2006), except that in the present work we allowed for non-isotropic orbit pole distribution. We used the following assumptions and approximations:

- Uniform distribution of orbit poles in $L_{\rm p}$ and in (a) $|\sin B_{\rm p}| = \sin B_{\rm x}$ to 1, or (b) $|\cos\epsilon| = \cos\epsilon_{\rm x}$ to 1, where $B_{\rm x}$ and $\epsilon_{\rm x}$ is a lower and upper limit cutoff of the distribution in ecliptic latitude and obliquity, respectively. For $B_{\rm x} = 0$ and $\epsilon_{\rm x} = 90^\circ$, it is the isotropic distribution.
- Zero eccentricity of the mutual orbit.
- Spherical shapes of both components.
- Same albedos for both components.
- Lommel-Seeliger scattering law for the distribution of apparent surface brightness over the disc (see Kaasalainen et al. 2002).
- Bulk density of 2.0 g/cm^3. The same bulk density is assumed for both components, i.e., the mass ratio is estimated as $(D_2/D_1)^3$.
- The probability of resolving mutual event is approximated with the step function given by eq. 8: $p_{\rm res} = 0$ and 1 for the relative brightness attenuation depth $F < 4\%$ and $\geq 4\%$ of total light, respectively.

Except for the assumed distribution of binary orbit poles, which is actually the characteristic that we were testing in this work, the assumptions and approximations given above are supported by the observational data for the binaries, or plausible ranges of deviations from them could not have significant effects in the simulations. For a discussion of a few effects that might not be entirely negligible see in Pravec et al. (2006).

As given in the first item above, we run the simulations for two variant distributions of binary orbit poles: (a) orbit poles concentrated towards the poles of the ecliptic and (b) orbit poles concentrated towards the poles of current osculating heliocentric orbits of binary systems. The case (a) may be more relevant, for following reasons: While being spun up by the YORP effect, the asteroid's pole moves towards the Cassini state 2 or 3, which both shift towards the poles of the ecliptic with the precession constant decreasing with increasing spin frequency. For non-zero inclination of the heliocentric orbit ($i_{\rm h}$), the asteroid's pole oscillates around the obliquity equal to $i_{\rm h}$ or $(180^\circ - i_{\rm h})$, though YORP alone would work towards more extreme obliquity values. See Sect. 6 for details and further discussion.

In each simulation, we randomly generated 30000 orbit poles with a chosen distribution in $|\sin B_{\rm p}|$ or $|\cos\epsilon|$. For each pole and each of the 18 binaries, we computed whether there occured mutual events (with relative attenuation depth $\geq 4\%$) for the first, discovery apparition epoch. If there occured an observable mutual event at the first apparition epoch, which is a requirement

for binary detection with our technique, then this case represents a positive detection of the binary in the first apparition. [2] For the positive detection, we then computed whether there occured an observable event also at the second, return apparition epoch. A resulted rate of occurence of positive re-detections in the return apparition for each of the 18 binaries was recorded. A result of the simulation for the assumed isotropic distribution of binary orbit poles (the null hypothesis) is shown in Table 3. There, $n_{\rm 1stapp}$ is a number of positive detections of the binary for the 30000 random orbit pole generations, $n_{\rm 2ndapp}$ is a number of positive re-detections of the $n_{\rm 1stapp}$ binaries detected in the 1st apparition, and the probability of a positive re-detection is given in the last column. [3] The median probability of positive re-detection for the 18 binaries is ~ 0.30.

After completing the simulation with the 30000 random generations for a given test distribution of orbit poles, we then used the resulted probabilities of positive re-detections and computed a probability density of getting $N_{\rm 2app}$ of positive re-detections of the 18 studied binaries. The probability density was computed by random generating positive/negative detections for the 18 binaries with the estimated individual probabilities ($n_{\rm 2ndapp}/n_{\rm 1stapp}$), repeated 10000 times. Relative frequencies of getting $N_{\rm 2app}$ positive re-detections of the 18 cases in the 10000 random generations were plotted in a histogram and the resulted probability density of positive re-detections was then compared to the observed number of 15 of the 18 binaries actually showing mutual events in their return apparitions.

The null hypothesis of the isotropic distribution of binary orbit poles ($B_{\rm x} = 0, \epsilon_{\rm x} = 90^\circ$) is rejected at a high confidence level. The simulation gave that an expected number of positive re-detections was 6 ± 3 (the 95% probability interval) and a probability of getting 15 positive re-detections among the 18 studied binaries was $< 10^{-4}$ (see Fig. 1).

The high observed number of positive re-detections indicates that there is a lack of binary orbit poles at low ecliptic latitudes (at obliquities around 90°) and that they concentrate at high ecliptic latitudes. To estimate how large is the concentration of orbit poles towards the poles of the ecliptic or, alternatively, towards the poles of current binary heliocentric orbits, we run the simulations for several trial distributions with poles distributed uniformly

[2] Here we assume that the probability $p_{\rm cov}$ of covering the mutual event with observations in the discovery apparition is independent of the orbit pole orientation. In fact it is not exactly so, as for non-central events, the event duration is shorter than for central ones, thus there may be a slight dependence of $p_{\rm cov}$ on orbit pole position. We neglect this minor effect in our simulations.

[3] For most of the binaries, the computed probability of a positive re-detection in the return apparition was in a range from 0.17 to 0.41 for the assumed isotropic distribution of binary orbit poles. Two of them, (2577) Litva and (5477) Holmes had, however, a higher probability of positive re-detection (0.74 and 0.80). This was because the return apparitions of the two binaries happened to be placed approximately diametrically opposite in their heliocentric orbits with respect to the discovery apparition, resulting in the enhanced probability of re-detection.

in the range $|\sin B_{\rm p}| = \sin B_{\rm x}$ to 1, and $|\cos\epsilon| = \cos\epsilon_{\rm x}$ to 1.

In Figs. 2 to 7, we present the resulted probability density distributions for $B_{\rm x}$ and $(90^\circ - \epsilon_{\rm x}) = 30^\circ, 45^\circ, 53^\circ, 60^\circ, 65^\circ$, and 70°. While for both $B_{\rm x}$ and $(90^\circ - \epsilon_{\rm x}) = 30^\circ$ we still get a probability of getting ≥ 15 positive re-detections of the 18 binaries to be low, $< 10^{-3}$ (Fig. 2), the probability becomes higher with increasing cutoff latitute and co-obliquity. For the test distribution concentrated towards the ecliptic poles, the probability is estimated to be 1%, 4%, 6% and 9% for the distribution cut at $B_{\rm x} = 53^\circ, 60^\circ$, 65° and 70°, respectively. For the alternative distribution of binary poles concentrated towards the heliocentric orbit poles, the probability is estimated to be 1%, 7%, and $> 15\%$ for the distribution cut at $(90^\circ - \epsilon_{\rm x}) = 45^\circ, 53^\circ, \geq 60^\circ$, respectively.

The simulations suggest that binary orbit poles concentrate within $\sim 30^\circ$ of the ecliptic poles, or alternatively, within $\sim 40^\circ$ of the heliocentric orbit poles. They do not distinguish which one of the two hypotheses —binary poles concentration in ecliptic latitude vs concentration in obliquity— is valid; a theoretical study of this problem is given in Sect. 6. We point out that the trial pole distributions with a step function at given ecliptic latitude or co-obliquity are arbitrary and that an actual distribution of binary orbit poles may be more gradual.

5 Estimated pole positions of binary asteroids

The available observations allowed us to derive models for the 18 studied binaries. Their estimated orbit poles are in a good agreement with the anisotropic distribution that we found with the simulations in the previous section. We point out that this binary asteroids sample is biased because of the discovery selection effects, see the binary detection theory in Sect. 2. We did not attempt to debias distributions of the estimated parameters of the binary sample directly, for following reasons: we did not get unique models for all the 18 binaries, and some estimated orbit poles have substantial uncertainties; the discovery selection effects are affected by limited coverage of surveyed objects (they had $p_{\rm cov} < 1$) that makes debiasing of the parameters of the sample of binaries more complex than the simulations presented in Sect. 4 where for the planned observations in the return apparitions we effectively set $p_{\rm cov} = 1$.

The models of the binary systems were derived using the technique of Scheirich and Pravec (2009). For the modeling, the observational data were reduced using the standard technique described in Pravec et al. (2006); a rotation lightcurve of the primary was fitted and subtracted from the data. In three cases, namely Pogson, Polonskaya and Litva, there was present also a second rotational lightcurve component with period different from $P_{\rm orb}$. Its character leads us to suspect that it belongs to a third body in the system, see our reasoning given in the discussions for the three asteroids below. To account for presence of the third body, a total light flux scattered towards observer

was computed as $I_1 + I_2 + I_3$, where I_i is the light flux from the i-th body. As we did not constrain I_3 from our observations (as we saw no mutual events involving the third body), we run our models for the three systems with a few values of I_3 in a range from 0 and I_1, i.e., sampling the size range of the suspect third body from negligible size up to a size equal to that of the primary. This way we estimated a sensitivity of our results on the size of the third body.

In the orbit model, shapes of the components were represented as ellipsoids — an oblate spheroid for the primary and a prolate spheroid for the secondary— orbiting each other on Keplerian orbit. The secondary was assumed to rotate synchronously and its long axis was aligned with the centers of the two bodies. Eccentricities of the mutual orbits were found to be small, from 0 up to an upper limit that reached values from 0.03 (for 1453 Fennia) up to 0.17 for the case of (4029) Bridges with the least constrained eccentricity. In modeling the eccentric orbit, a precession of the line of apsides was computed. A pericenter drift rate depends on primary's polar flattening (see Murray and Dermott 1999, eq. 6.249) that was only poorly estimated from our observations —the primary's axial ratio a_1/c_1 was constrained to be in a range from 1 up to a certain upper limit in most cases— we fitted the pericenter drift rate as an independent parameter. Its initial values were stepped in a range from zero to 30°/day; this range encompasses all possible values for the flattening and other parameters of the modeled binaries. To reduce a complexity of the modeling, the upper limit on eccentricity was estimated by fitting data from the best-covered apparition only. In modeling data from all apparitions together, zero eccentricity was assumed.

We summarize our results in Table 1. In the following paragraphs, we comment on the results for the systems where we got a unique solution and for the two cases of (2006) Polonskaya and (2044) Wirt where we obtained two possible solutions but which are among the three cases where we did not see mutual events in the return apparition.

(1338) Duponta

We observed this binary in two apparitions: from 2007-03-06.8 to 2007-04-22.9, and from 2010-01-04.9 to 2010-03-09.9.

We found a unique solution for both the pole and period of the mutual orbit, fitting our model to the data for the orbital lightcurve component from both apparitions simultaneously. The estimated orbit period is $P_{\rm orb} = (17.5680 \pm 0.0001)$ h. Limiting values of the ecliptic coordinates for the admissible area of the orbit pole are given in Table 1 and the area is plotted in Fig. 8. An upper limit on flattening of the primary modeled as an oblate spheroid is $a_1/c_1 = 3.3$. The best-fit value of a_1/c_1 is 1.1, and the quality of the fit decreases with increasing a_1/c_1, so the lower values are preferred. An upper limit on the eccentricity, derived from data of the best covered apparition 2007, is 0.14. All the uncertainties and admissible ranges of the parameters correspond to 3σ confidence level (see Scheirich and Pravec 2009).

Examples of the orbital lightcurve component together with the synthetic lightcurve for the best-fit solution are presented in Fig. 9.

(1453) Fennia

We observed this binary in three apparitions: from 2007-11-04.3 to 2007-12-02.3, from 2009-08-14.4 to 2009-08-27.8, and from 2011-01-28.9 to 2011-04-29.9.

We found a unique solution for both the pole and period of the mutual orbit, fitting our model to the data for the orbital lightcurve component from both apparitions simultaneously. The estimated orbit period is $P_{\rm orb} = (23.00351 \pm 0.00005)$ h. Limiting values of the ecliptic coordinates for the admissible area of the orbit pole are given in Table 1 and the area is plotted in Fig. 10. Lower and upper limits on flattening of the primary modeled as an oblate spheroid are $a_1/c_1 = 1.4$ and 2.4, respectively. An upper limit on the eccentricity, derived from data of the best covered apparition 2011, is 0.03. All the uncertainties and admissible ranges of the parameters correspond to 3σ confidence level (see above).

Examples of the orbital lightcurve component together with the synthetic lightcurve for the best-fit solution are presented in Fig. 11.

(1830) Pogson

We observed this system in three apparitions: from 2007-04-18.4 to 2007-06-06.6, from 2008-09-02.8 to 2008-11-06.8, and from 2010-02-20.6 to 2010-04-08.7.

In all the three apparitions, the lighcurve data revealed two rotational components with superimposed mutual events. The two rotational components have periods of (2.57003 ± 0.00006) h and (3.2626 ± 0.0004) h (the uncertainties are 1σ) with apparent amplitudes of 0.10–0.12 and 0.03 mag, respectively. Both rotational components are present at all orbital phases including mutual events, with unchanged shape in the event. The fact that the second rotational component does not disappear in mutual events indicates that it is not a rotation of the secondary. We consider that it may rather belong to a third body in the system. This proposed explanation will have to be confirmed and a size and distance of the third body will have to be estimated with future observations.

We found a unique solution for both the pole and period of the mutual orbit, fitting our model to the data for the orbital lightcurve component, derived with subtracting both rotational components, from all the three apparitions simultaneously. The estimated period is $P_{\rm orb} = (24.24580 \pm 0.00006)$ h. Limiting values of the ecliptic coordinates for the admissible area of the orbit pole are given in Table 1 and the area is plotted in Fig. 12. An upper limit on flattening of the primary modeled as an oblate spheroid is $a_1/c_1 = 3.4$. The

best-fit value of a_1/c_1 is 1.3, and the quality of the fit decreases with increasing a_1/c_1, so the lower values are preferred. An upper limit on the eccentricity, derived from data of the best covered apparition 2008, is 0.10. All the uncertainties and admissible ranges of the parameters correspond to 3σ confidence level (see above).

We analysed an effect of possible presence of the third body on our modeling and estimated parameters. The size ratio $D_2/D_1 = 0.30 \pm 0.02$ that was estimated from the depth of the secondary mutual event becomes a lower limit if there is a third body contributing to the total light of the system. Thus, in addition to running our orbit modeling with the size ratio estimate of 0.30 that corresponds to a zero or negligible size of the third body, we run the model also for a few cases with the third body having a diameter in the range from zero up to D_1. We found that the presence of the third body had a negligible effect on the estimated orbit period, but it affected the estimated orbit pole area. The admissible area of the pole shrinks by up to a factor of three with the third body's diameter increasing up to the diameter of the primary (see Fig. 12).

Examples of the orbital lightcurve component together with the synthetic lightcurve for the best-fit solution are presented in Fig. 13.

(2006) Polonskaya

We observed this system in three apparitions: from 2005-11-01.0 to 2005-12-07.1, from 2008-06-04.3 to 06.4, and from 2010-01-10.1 to 2010-02-22.3. Mutual events were observed in the first and the third apparition only. In the second apparition, we covered 61% of the orbit and there did not occur mutual events width depth greater than 0.02 mag.

In all the three apparitions, the lighcurve data revealed two rotational components (with superimposed mutual events in the first and the third apparition). The two rotational components have periods of (3.11809 ± 0.00007) h and (6.6593 ± 0.0004) h (the uncertainties are 1σ) with apparent amplitudes of 0.08–0.10 and 0.07–0.10 mag, respectively. Both rotational components are present at all orbital phases including mutual events, with unchanged shape in the event. The fact that the second rotational component does not disappear in mutual events indicates that it is not a rotation of the secondary. We consider that it may rather belong to a third body in the system. This proposed explanation will have to be confirmed and a size and distance of the third body will have to be estimated with future observations.

Combining data from the first and the last apparitions, we found five solutions for the period and two solutions for the pole of the mutual orbit, fitting our model to the data for the orbital lightcurve component, derived with subtracting both rotational components. The estimated periods are $P_{\rm orb} = 19.1407$ h, 19.1507 h, 19.1553 h, 19.1607 h and 19.1654 h, with 3-σ errors 0.0001–0.0002 h. Limiting values of the ecliptic latitudes for the admissible areas of the orbit

pole are $B_{\rm p} > +54^\circ$ and $< -60^\circ$ (for model bulk density > 1.0 g cm^{-3} the values of $B_{\rm p}$ are constrained to be $> +71^\circ$ and $< -72^\circ$).

An attempt to join in the data from the 2008 apparition where there occured no event deeper than 0.02 mag failed; for all the solutions from the 2005+2010 data, there were predicted observable events to occur during the times of the 2008 observations. This leads us to consider that some assumption of the model might not hold. In particular, it is possible that the mutual orbit plane of the components was not constant and that it precessed. If so, then the joint solution of the 2005 and 2010 observations may be spurious.

(2044) Wirt

We observed this binary in three apparitions: from 2005-11-29.8 to 2006-01-29.9, from 2008-08-22.3 to 26.3, and from 2010-03-07.3 to 04-19.8. Mutual events were observed in the first apparition only. In the two return apparitions, there did not occur mutual events width depth greater than 0.03 mag.

We found two solutions for the pole and period of the mutual orbit, fitting our model to the data for the orbital lightcurve component from the first apparition. The estimated orbit periods are $P_{\rm orb} = (18.976 \pm 0.005)$ h and (18.965 ± 0.006) h. Limiting values of the ecliptic coordinates for the admissible areas of the orbit pole are given in Table 1 and the areas are plotted in Fig. 14. For both solutions, there occur no mutual events in the two return apparitions, consistent with the observations.

An upper limit on flattening of the primary modeled as an oblate spheroid is $a_1/c_1 = 1.5$. An upper limit on the eccentricity is 0.10. All the uncertainties and admissible ranges of the parameters correspond to 3σ confidence level (see above).

Examples of the orbital lightcurve component together with the synthetic lightcurves for the two best-fit solutions are presented in Fig. 15.

(2577) Litva

We observed this system in two apparitions: from 2009-02-28.1 to 2009-04-01.9, and from 2010-07-16.2 to 2010-08-31.3.

In both apparitions, the lighcurve data revealed two rotational components with superimposed mutual events. In the 2010 apparition, the two rotational components had periods of 2.8129 h and 5.6818 h with predominating uncertainties due to the synodic-sidereal effect that were estimated to be about 0.0001 h and 0.0004 h, respectively. In the 2009 apparition when there was a larger synodic-sidereal effect (about 0.0003 h and 0.002 h, respectively), the two periods were 2.8126 h and 5.684 h. Apparent amplitudes of the two rotational components were 0.17 and 0.06 mag at solar phases 11°–22° in 2010, while they were somewhat greater, 0.24 and 0.09 mag at higher solar phases of

22°–30° in the 2009 apparition. Inspecting the behavior of the rotational components in the 2009 data where the mutual events were covered thoroughly, we found that both components were present at all orbital phases including mutual events, with apparently unchanged shape in the event. The fact that the second rotational component does not disappear in mutual events indicates that it is not a rotation of the secondary. Like in the similar cases of (1830) Pogson and (2006) Polonskaya, we consider that the second rotational component may rather belong to a third body in the system. This proposed explanation will have to be confirmed and a size and distance of the third body will have to be estimated with future observations.

We found a unique solution for both the pole and period of the mutual orbit, fitting our model to the data for the orbital lightcurve component, derived with subtracting both rotational components, from both apparitions simultaneously. The estimated period is $P_{\rm orb} = (35.8723 \pm 0.0008)$ h. Limiting values of the ecliptic coordinates for the admissible area of the orbit pole are given in Table 1 and the area is plotted in Fig. 16. An upper limit on flattening of the primary modeled as an oblate spheroid is $a_1/c_1 = 2.3$. An upper limit on the eccentricity, derived from data of the best covered apparition 2009, is 0.08. All the uncertainties and admissible ranges of the parameters correspond to 3σ confidence level (see above).

We analysed the effect of possible presence of the third body on our modeling and estimated parameters. From the depth of the mutual events observed in 2009, we estimated the size ratio $D_2/D_1 = 0.34 \pm 0.02$. Analogously with the case of (1830) Pogson, in addition to running our orbit modeling with the size ratio estimate of 0.34 that corresponds to a zero or negligible size of the third body, we run the model also for a few cases with the third body having a diameter in the range from zero up to D_1. We found that the presence of the third body had a negligible effect on the estimated orbit period and only a small effect on the estimated orbit pole area; the admissible area of the pole shrinks by $\sim 20\%$ with the third body's diameter increasing up to the diameter of the primary (see Fig. 16).

Examples of the orbital lightcurve component together with the synthetic lightcurve for the best-fit solution are presented in Fig. 17.

(2754) Efimov

We observed this binary in three apparitions: from 2006-08-14.1 to 2006-11-18.1, from 2008-03-09.1 to 2008-03-13.3, and from 2011-01-30.8 to 2011-03-07.0.

In the 2nd apparition of March 2008 the asteroid was placed almost precisely (within a few degrees) diametrically opposite in its heliocentric orbit with respect to the discovery apparition. As such, the 2nd apparition's data would provide negligible constraints in the simulations presented in Section 4 and therefore this 2008 apparition was not counted as a fully-fledged return ap-

parition for the purpose of the survey simulations. Instead, we took the 2011 apparition as the return apparition, see the entry in Table 2. Nonetheless, the 2008 data were useful in the orbit modeling presented here.

We found a unique solution for both the pole and period of the mutual orbit, fitting our model to the data for the orbital lightcurve component from all the three apparitions simultaneously. The estimated orbit period is $P_{\rm orb} = (14.77578 \pm 0.00008)$ h. Limiting values of the ecliptic coordinates for the admissible area of the orbit pole are given in Table 1 and the area is plotted in Fig. 18. An upper limit on flattening of the primary modeled as an oblate spheroid is $a_1/c_1 = 1.8$. The best-fit value of a_1/c_1 is 1.1, and the quality of the fit decreases with increasing a_1/c_1, so the lower values are preferred. An upper limit on the eccentricity, derived from data of the best covered apparition 2006, is 0.08. All the uncertainties and admissible ranges of the parameters correspond to 3σ confidence level (see above).

Examples of the orbital lightcurve component together with the synthetic lightcurve for the best-fit solution are presented in Fig. 19.

(3309) Brorfelde

We observed this binary in three apparitions: from 2005-10-25.1 to 2005-11-03.4, from 2009-01-28.1 to 2009-04-02.1, and from 2010-10-07.9 to 2010-12-26.3.

We found a unique solution for both the pole and period of the mutual orbit, fitting our model to the data for the orbital lightcurve component from all the three apparitions simultaneously. The estimated orbit period is $P_{\rm orb} = (18.46444 \pm 0.00003)$ h. Limiting values of the ecliptic coordinates for the admissible area of the orbit pole are given in Table 1 and the area is plotted in Fig. 20. An upper limit on flattening of the primary modeled as an oblate spheroid is $a_1/c_1 = 2.1$. The best-fit value of a_1/c_1 is 1.3, and the quality of the fit decreases with increasing a_1/c_1, so the lower values are preffered. An upper limit on the eccentricity, derived from data of the best covered apparition 2010, is 0.08. All the uncertainties and admissible ranges of the parameters correspond to 3σ confidence level (see above).

Examples of the orbital lightcurve component together with the synthetic lightcurve for the best-fit solution are presented in Fig. 21.

(4029) Bridges

We observed this binary in three apparitions: from 2006-04-11.4 to 2006-05-04.8, from 2007-10-05.0 to 2007-11-12.1, and from 2010-05-08.4 to 2010-06-09.2.

We found a unique solution for both the pole and period of the mutual orbit, fitting our model to the data for the orbital lightcurve component from all

the three apparitions simultaneously. The estimated orbit period is $P_{\rm orb} = (16.31701 \pm 0.00004)$ h. Limiting values of the ecliptic coordinates for the admissible area of the orbit pole are given in Table 1 and the area is plotted in Fig. 22. An upper limit on flattening of the primary modeled as an oblate spheroid is $a_1/c_1 = 3.5$. An upper limit on the eccentricity, derived from data of the best covered apparition 2006, is 0.17. All the uncertainties and admissible ranges of the parameters correspond to 3σ confidence level (see above).

Examples of the orbital lightcurve component together with the synthetic lightcurve for the best-fit solution are presented in Fig. 23.

(5477) Holmes

We observed this binary in two apparitions: from 2005-11-02.1 to 2005-12-09.0, and from 2007-05-26.3 to 2007-07-12.6.

We found a unique solution for both the pole and period of the mutual orbit, fitting our model to the data for the orbital lightcurve component from both apparitions simultaneously. The estimated orbit period is $P_{\rm orb} = (24.4036 \pm 0.0002)$ h. Limiting values of the ecliptic coordinates for the admissible area of the orbit pole are given in Table 1 and the area is plotted in Fig. 24. An upper limit on flattening of the primary modeled as an oblate spheroid is $a_1/c_1 = 2.0$. The best-fit value of a_1/c_1 is 1.2, and the quality of the fit decreases with increasing a_1/c_1, so the lower values are preferred. An upper limit on the eccentricity, derived from data of the best covered apparition 2005, is 0.05. All the uncertainties and admissible ranges of the parameters correspond to 3σ confidence level (see above).

Examples of the orbital lightcurve component together with the synthetic lightcurve for the best-fit solution are presented in Fig. 25.

(6084) Bascom

We observed this binary in two apparitions: from 2005-12-29.5 to 2006-02-09.7, and from 2008-08-24.6 to 2008-09-10.6. In the return apparition, there did not occur mutual events width depth greater than 0.02 mag.

We found a unique solution for both the pole and period of the mutual orbit, fitting our model to the data for the orbital lightcurve component from the first apparition. The lack of mutual events in the return apparition did not constrain the solution further; for all poles within the area derived from the first apparitions, there do not occur events for the geometry of the return apparition. The estimated orbit period is $P_{\rm orb} = (43.51 \pm 0.02)$ h. Limiting values of the ecliptic coordinates for the admissible area of the orbit pole are given in Table 1 and the area is plotted in Fig. 26. An upper limit on flattening of the primary modeled as an oblate spheroid is $a_1/c_1 = 2.9$. An upper limit on the eccentricity is 0.15. All the uncertainties and admissible ranges of the parameters correspond to 3σ confidence level (see above).

Examples of the orbital lightcurve component together with the synthetic lightcurve for the best-fit solution are presented in Fig. 27.

6 Interpretation and Discussion

Binary systems among small asteroids (primary diameters $D_1 \lesssim 10$ km) appear to form from parent bodies spinning at a critical rate by some sort of fission or mass shedding process (Scheeres 2007, Pravec and Harris 2007, Walsh et al. 2008). A mechanism to spin the parent asteroid up to its critical rotation frequency is provided by the Yarkovsky-O'Keefe-Radzievskii-Paddack (YORP) effect (e.g., Bottke et al. 2006). While spinning it up, the YORP effect also changes the asteroid's spin orientation substantially toward a YORP end state (see, e.g., Čapek and Vokrouhlický 2004). Thus, by reaching the critical spin frequency the parent bodies may get an anisotropic distribution of spin orientations with poles concentrating near the YORP asymptotic states. After the formation of a binary, the primary component may experience a further evolution by YORP, again toward a YORP end state. An additional mechanism affecting orbits of binary asteroids are gravitational perturbations from Sun.

We consider three hypotheses for origin of the anisotropic distribution of binary orbit poles:

(1) The preferentially up/down-right orientation of binary orbit poles is set up upon their formation, i.e., it reflects orientations of spin vectors of their parent bodies with poles evolved toward the YORP asymptotic states near 0 and 180°.
(2) Binaries formed with a broader distribution of orbit poles but later they were YORP-tilted towards the YORP asymptotic states.
(3) Binaries with poles close to the ecliptic plane were eliminated or transferred to higher ecliptic latitudes by a gravitational dynamical process.

In Section 6.1 below we examine a short-term dynamical evolution of binary asteroids with a numerical model, showing that it does not support the hypothesis 3 above. In Section 6.2 we then briefly discuss the hypotheses 1 and 2.

6.1 Short-term dynamical evolution: a simple numerical model

At the first sight, the reported situation is reminiscent of irregular satellites of giant planets, whose inclination relative to the ecliptic plane also avoids values around the polar orbit. In that case, the solar-tide perturbation has been found to drive large oscillations of the satellite eccentricity and inclination in the non-populated inclination region, the process generally known as the Kozai dynamics (e.g. Kozai 1962, Carruba et al. 2002, Nesvorný et al. 2003).

Eventually, the pericenter distance would have been too small and impacts on regular satellites of the planet would occur.

Here, however, the situation is different and the observed satellites in the binary systems are analogs of the regular, rather than irregular, satellites of giant planets. This is because of their close proximity to the primary. Assuming reasonable flattening of the latter, in quantitative terms $\gamma = c_1/a_1 \leq 0.97$ where c_1 and a_1 are polar and mean equatorial radii of the dynamically equivalent ellipsoid (i.e., ellipsoid with the same moments of inertia) of the primary (see Appendix), the Laplace plane of the satellite motion tilts from the ecliptic to the equatorial plane of the primary for distances smaller than several tens of primary radii[4] (e.g., Goldreich 1965, Mignard 1981). This means that the quadrupole perturbation due to the primary oblateness dominates the solar-tide effect. In particular, it drives fast pericenter circulation which effectively inhibits the Kozai mechanism. As a result the whole binary system acts as a single gyroscope on a heliocentric orbit. The latitude variations of its angular momentum may still be non-trivial, due to interaction with the precession of the heliocentric orbit of the binary, but overall no major dynamical instability at low ecliptic latitudes is expected.

In order to verify the picture outlined in the previous paragraphs, we constructed a simple numerical model that tracks orbital evolution of the satellite and the spin of the primary. The assumptions make the model valid only over a short timespan of $\simeq$ My, but it still provides a basic tool to verify binary orbital pole stability at low ecliptic latitudes; note that the Kozai instability timescale is much shorter, several thousands of years only. Formulation and basic features of the model are given in the Appendix. In what follows we provide three different examples of a short-term orbital evolution for binaries from our observed sample.

Low-inclination, main belt binary: (4029) Bridges. First, we choose the case of (4029) Bridges residing on low-inclination, main belt heliocentric orbit. Because it is located outside the 3/1 mean motion resonance with Jupiter, the proper frequency of nodal precession is rather large, $s \simeq -51.8$ arcsec/yr, while the proper inclination is only moderate $\simeq 5.9^\circ$. Its contribution is well separated from the forced term at $s_6 \simeq -26.3$ arcsec/yr frequency and only $\simeq 1^\circ$ amplitude in the Fourier spectrum of the non-singular inclination vector $\zeta = q + \imath p = \sin I/2 \exp(\imath\Omega)$ of the heliocentric orbit.

Figure 28 shows a sample of orbit-pole evolutions for various initial latitudes and longitudes equal to $\Omega + 90^\circ$ (left panel) and $\Omega + 270^\circ$ (right panel); Ω is the longitude of ascending node of the heliocentric orbit. Additionally, the evolution shown by the thick curve on the left panel corresponds to the initial pole position $(L_\mathrm{p}, B_\mathrm{p}) = (305^\circ, -85^\circ)$ very close to the osculating pole of

[4] The distance from the primary at which solar-tide effects take over the primary oblateness effect can be estimated by $d_2 \simeq [2\,(C-A)\,a_\mathrm{h}^3/m_0]^{1/5}$, where A and C are equatorial and polar moments of inertia of the primary, a_h is the semimajor axis of the binary's heliocentric orbit and m_0 the solar mass.

the heliocentric orbit and near the center of the uncertainty region of the solution (Fig. 22). For any initial latitude value the evolution is very stable, showing only very small oscillations driven by solar torque on the system and small heliocentric orbit inclination with respect to the ecliptic. This is because the effective precession constant of the system, see Eq. (10) below, is $\simeq 20$ arcsec/yr, well separated from both s and s_6 terms in ζ.

High-inclination, Hungaria binary: (1453) Fennia. Next, we consider the case of Hungaria-type binary (1453) Fennia, residing on high-inclination heliocentric orbit. In this case the spectrum of ζ is dominated by the proper term with frequency $s \simeq -20.4$ arcsec/yr and proper inclination of $\simeq 24.4°$, but there are more planetary terms with similar frequencies. Of particular interest may be the $s_4 \simeq -17.8$ arcsec/yr with forced inclination $\simeq 0.4°$ and the $s_6 \simeq -26.3$ arcsec/yr with forced inclination $\simeq 0.2°$.

Figure 29 shows the same numerical experiment as above for (4029) Bridges, notably a short numerical integration of the Fennia system with different initial latitude values of its orbit pole. The thick curve on the right panel shows a possible evolution of the orbit pole for this binary for initial position $(L_\mathrm{p}, B_\mathrm{p}) = (95°, -66°)$ very close to the osculating pole of the heliocentric orbit and near the center of the uncertainty region of our solution (Table 1 and Fig. 10). Here we see a much different picture, with individual tracks of the orbit pole showing large oscillations, especially for positive latitude value (prograde sense of binary motion). Since these oscillations are significantly larger than the proper inclination value of the heliocentric orbit, the situation warrants a closer analysis.

Our results obviously confirm that: (i) the primary's oblateness efficiently locks the satellite orbit to its equatorial plane, and (ii) the satellite orbit maintains to be quasi-circular (with only very small oscillations of the osculating eccentricity value). Henceforth, the Kozai mechanism is inhibited for any initial value of orbit pole, even if in the ecliptic plane ($B_\mathrm{p} = 0°$). Rotation of the primary and revolution of the satellite thus couple together and act as a single gyroscope with the angular momentum composed of the two contributions. In order to understand the general pattern of its ecliptic-latitude evolution from Fig. 29, one must determine the appropriate precession constant α of the system.

For a single asteroid, rotating about the principal axis of the inertia tensor we have

$$\alpha_\mathrm{prim} = \frac{3}{2}\frac{n_\mathrm{h}^2}{\omega}\frac{C-A}{C} \,, \tag{9}$$

where n_h is the mean motion of the heliocentric revolution, ω is the angular rotation frequency, C and A are the principal moments of the inertia tensor about the polar and equatorial axes (e.g., Bertotti et al. 2003). However, the presence of the satellite modifies the situation. The gravitational torque due to the Sun now acts both on the primary and the satellite orbit. The precession

constant of the whole binary system thus reads (e.g., Ward 1975, French et al. 1993)

$$\alpha_{\rm eff} = \frac{3}{2}\frac{n_{\rm h}^2}{\omega}\frac{J_2+q}{\lambda+l}\ , \tag{10}$$

where $J_2 = (C-A)/(m_1R_1^2)$, $\lambda = C/(m_1R_1^2)$, $q = m_2a_{\rm orb}^2/(2m_1R_1^2)$ and $l = m_2a_{\rm orb}^2 n_{\rm b}/(m_1R_1^2\omega)$ (with m_1 mass of the primary and R_1 its effective radius, m_2 mass of the satellite and $a_{\rm orb}$ semimajor axis of the satellite orbit; see Appendix for more details). Here, respectively, q is the effective contribution of the satellite orbit to the dynamical flattening measured by the quadrupole coefficient J_2, and l is the orbital angular momentum of the satellite relative to the rotational angular momentum of the primary. We note that l is typically a small contribution to λ in the denominator of Eq. (10), meaning most of the angular momentum is in the rotation of the primary. On the contrary, unless very large oblateness of the primary, q dominates contribution of J_2 in the numerator of Eq. (10). In conclusion, the precession constant of the binary system is larger than that of solitary primary as a result of the satellite presence. For (1453) Fennia, for instance, we would have $\alpha_{\rm prim} \simeq 14.9$ arcsec/yr for the primary only (assuming oblateness $\gamma = c_1/a_1 = 0.89$, cf. Appendix), but the true value according to Eq. (10) with data in Table 1 is $\alpha_{\rm eff} \simeq 85$ arcsec/yr. This is a much larger frequency, which has subtle implications. For instance, the primary's precession constant would imply only two proper-frequency Cassini states [5] at high latitudes. However, the true system with larger $\alpha_{\rm eff}$ value has four proper-frequency Cassini states, with the Cassini state 2 at only $\simeq 36^\circ$ latitude (Fig. 29, left panel). Also the newly bifurcated Cassini state 1 is at $\simeq 58^\circ$ latitude and longitude offset by 270° from the longitude of ascending node of Fennia's heliocentric orbit (Fig. 29, right panel). Orbit pole evolution may oscillate about these states with large amplitude. The solutions for initially retrograde poles show a much more regular evolution with the amplitude of latitude oscillations basically given by the inclination of the binary's heliocentric orbit.

High-inclination, main belt binary: (2044) Wirt. Finally, we consider the case of (2044) Wirt, residing on high-inclination orbit with semimajor axis value in the inner part of the main belt. In fact, with its mean perihelion at $\simeq 1.65$ AU only (and osculating value reaching down to $\simeq 1.42$ AU), this asteroid is on an escaping route to the planet crossing zone. The spectrum of ζ is dominated by the proper-frequency term with $s \simeq -43.3$ arcsec/yr and about $\sim 23.5^\circ$ proper inclination amplitude, but it also contains a large number of contributions from the forced planetary frequencies and their linear combinations with s (all having amplitudes of $\simeq 2.2^\circ$ and smaller).

Figure 30 shows again a sample of possible pole evolutions with different initial orientations, including those that start near the middle of our two solutions

[5] Detailed discussion of the Colombo top model and Cassini states can be found in Colombo (1966), Henrard and Murigande (1987) or Vokrouhlický et al. (2006).

from Table 1 and Fig. 14 (shown as thick curves). The general behavior of the solutions can again be understood in terms of a modification of precession constant due to the satellite: assuming a polar oblateness $\gamma = c_1/a_1 = 0.75$ of the primary, we would have $\alpha_{\rm prim} \simeq 13.3$ arcsec/yr that becomes $\alpha_{\rm eff} \simeq 33.7$ arcsec/yr with the satellite (for smaller oblateness values, larger γ, both $\alpha_{\rm prim}$ and $\alpha_{\rm eff}$ are smaller, but the gross results are not changed unless $\gamma > 0.9$). The $\alpha_{\rm eff}$ value is large enough to significantly displace Cassini state 2, especially since (2044) Wirt has a high inclination of the heliocentric orbit, to $\simeq 46^\circ$ distance from the heliocentric orbit pole. This puts the Cassini state 2 at $\simeq 67^\circ$ ecliptic latitude, right in the zone of our prograde solution for this system (see the thick curve on the left panel of Fig. 30). An exact location at the Cassini state 2 would also require 180° longitude difference between the pole of the heliocentric orbit and the binary pole; we find that our prograde solution is only $\sim 40^\circ$ away, implying a small amplitude circulation about the Cassini state 2. Smaller polar oblateness values for the primary would displace the Cassini state 2 to slightly higher ecliptic latitude value and would imply larger amplitude oscillation of the orbit pole of (2044) Wirt. The high-inclination and high-eccentricity state of the Wirt heliocentric orbit, with occasional crossing of the Mars orbit, makes the behavior of ζ only quasi-periodic. Its truncated Fourier representation is only approximate and includes unusual prograde precessing terms which produce long-period variations in the pole latitude of our solutions near $B_{\rm p} \simeq -50^\circ$.

We conclude that while the examples of Hungaria-type binary, (1453) Fennia, and Phocaea-type binary, (2044) Wirt, above show that latitude of the orbit pole may have non-trivial evolution, they do not provide evidence for larger stability at high latitudes versus low latitudes. On the contrary: if we were to run orbit pole evolutions for denser and initially isotropic distribution, we would obtain a homogeneous occupation of any latitude (in $\cos B_{\rm p}$ measure) over a time. This experiment has been performed by Vokrouhlický et al. (2006) for single asteroids, but as we proved that the compact binaries effectively behave like single objects with only modified precession constant, it applies also here. We thus conclude, that for the observed parameters of the binary systems, their dynamics is stable over a My timescale even for very small ecliptic latitudes of the orbital pole. Assuming an initially isotropic distribution of poles, it should remain an isotropic distribution at any moment of time.

While the pole stability at all latitudes is true population-wise, we return to the issue of possibly complicated latitude tracks of individual objects with very large oscillations in the prograde zone. This especially applies to binaries which have large inclination value of their heliocentric orbit with respect to the ecliptic; notable examples are Hungaria and Phocaea groups (see Vokrouhlický et al. 2006). In these cases, the latitude value of the current orbit pole position of the binary may not directly reflect its initial value. Only a more detailed information about the system, such as a constraint on the polar flattening of the primary, would provide more insight in the possible evolutionary tracks of the pole.

Our numerical model provides an information about the observed binary systems over a timescale which might be only a snapshot in their lifetime. While, the observed (tidal) synchronization of the satellite's rotation implies ages longer than $\sim (1-10)$ My (e.g., Taylor and Margot 2010, 2011), we have only a loose handle of the upper age limit. The collisional lifetime of the km-size satellites suggests that most of the binary systems in our sample are not older than $\sim$ (200 − 500) My (e.g., Bottke et al. 2005) and a similar, or longer, timescale is obtained by non-synchronization of the rotation rate of the primary. This is a long time, over which weak torques like the YORP effect might act on the systems. For instance, distribution of the spin orientations of single asteroids is skewed toward the ecliptic poles in a good agreement with a steady-state model with the YORP effect (e.g., Hanuš et al. 2011). In the same way, YORP acting on the primary component should slowly tilt the system toward the asymptotic YORP states, presumably at large ecliptic latitudes.

Using data in Čapek and Vokrouhlický (2004) we find that near-critically rotating $\simeq 8$ km asteroid in the inner part of the main belt should tilt its pole position by $\simeq 10^\circ$ per 100 My on average. Because of the $\propto 1/D^2$ scaling of the YORP strength, a smaller body of $\simeq 4$ km size would have an average polar tilt of $\simeq 40^\circ$ per 100 My. Thus, if binary systems are typically old (ages $\gtrsim 10^8$ yr), their poles might have been further evolved towards the YORP asymptotic states during their lifetime.

In conclusion, we consider that the concentration of binary orbit poles on high ecliptic latitudes reflects primarily their *preferential formation* at these states (the hypothesis 1 above). As mentioned in the first paragraph of this Section 6, during the YORP spin up of parent bodies to the critical fission frequency, their spin orientations should be substantially YORP-tilted toward the YORP asymptotic states. A possible contribution of the additional process of further evolution of a primary spin by YORP during the binary's life will need to be studied.

Acknowledgements

The work at Ondřejov and the Charles University Prague was supported by the Grant Agency of the Czech Republic, Grants 205/05/0604 and 205/09/1107, and by the Research Programs MSM0021620860 and MEB0810085 of the Czech Ministry of Education. A.W.H. was supported by NASA grant NNX 09AB48G and by National Science Foundation grant AST-0907650. Observations at the Carbuncle Hill Observatory and the Hunters Hill Observatory were supported by a Gene Shoemaker NEO Grant from the Planetary Society. The work at Modra Observatory was supported by the Slovak Grant Agency for Science VEGA, Grants 2/0016/09 and 1/0636/09. The work at Skalnaté Pleso Observatory has been supported by the Slovak Grant Agency for Science VEGA, Grant 2/0022/10. Support for PROMPT has been provided by the National Science Foundation under awards CAREER-0449001, AAG-0707634, and MRI-0836187. O.V., P.L.-P. and A.T. would like to thank the staff of Cerro Tololo and Las Campanas Observatories in Chile, the Chilean Time Allocation Committee and the Instituto de Astronomia of the Universidad Catolica del Norte for continuous support for the observing runs in Chile. Funding for observations at the Palmer Divide Observatory was provided by NASA grant NNX10AL35G, by National Science Foundation grant AST-1032896, and by a 2007 Gene Shoemaker NEO Grant from the Planetary Society. F.M. was supported by the National Science Foundation under award number AAG-0807468.

APPENDIX

A Numerical model of binary's short-term evolution

In order to verify our conclusions from Sec. 6 we constructed a very simple numerical model to track orbital evolution of the binary system coupled with the spin evolution of the primary. The major simplifying assumptions are (i) a point-mass representation of the secondary component (the satellite), and (ii) an axisymmetric representation of the primary component in the binary system. Masses of the primary and secondary components are denoted m_1 and m_2; we also define dimensionless factors $X_1 = m_1/(m_1 + m_2)$ and $X_2 = m_2/(m_1 + m_2)$, which correspond to their respective contributions to the total mass of the binary system. [6] The primary is assumed to be an oblate spheroid [7] with the equatorial and polar axes denoted by a_1 and c_1, such that $\gamma = c_1/a_1 \leq 1$. Denoting $R_1 \simeq a_1\gamma^{1/3}$ the characteristic radius of the primary, defined as a radius of a sphere with the same volume, and using R_1 as the scaling parameter of the representation of primary's gravitational field, we have $J_2 \simeq 0.2\,(1-\gamma^2)\,\gamma^{-2/3}$ for its quadrupole parameter. We could also determine similar formulas for higher-degree zonal coefficients, but we shall not need them. Description of the evolution of the primary's spin axis also requires $(C-A)/C \simeq 0.5\,(1-\gamma^2)$, where C and A are polar and equatorial moments of inertia. Photometric observations of the primary components in binaries, including those in this paper, all suggest a small amplitude of the lightcurve from which we may estimate the ratio of the equatorial axis is unity within $\simeq 10-20\%$ accuracy. Radar observations also support this conclusion and additionally suggest only modest polar flattening with $\gamma \simeq 0.8-0.9$ (e.g., Ostro et al. 2006, Shepard et al. 2006, Taylor et al. 2008, Benner et al. 2010). The mutual gravitational interaction of the primary and secondary components is represented in our model to the quadrupole level of the primary's zonal field; while we could have taken higher-degree zonal terms into account, they would not bring new qualitative features in our analysis.

On the contrary, we need to take into account effects of the solar gravity for the binary dynamics. We use description in Jacobi coordinates, where $\mathbf{r}$ denotes relative position vector of the secondary with respect to the primary and $\mathbf{R}$ denotes relative position vector of the Sun with respect to the center of mass of the binary. Since our prime concern is the evolution of $\mathbf{r}$, and the relative velocity $d\mathbf{r}/dt$, we represent $\mathbf{R}$ with a simple elliptic orbit. Because the secular evolution of the binary orbit plane may be coupled to the corresponding secular evolution of the heliocentric orbit plane of the binary's center-of-mass motion, we only pay some attention in representation of its inclination I and

[6] Masses of both components were computed from the estimated sizes in Table 1 and a bulk density of 2.5 g/cm^3.

[7] The exact nature of the shape is, however, not a very restrictive assumption. As mentioned above, the major approximation in our model is the axial symmetry of the primary.

longitude of ascending node Ω. In particular, we use a Fourier representation of the non-singular inclination vector $\zeta = q + \imath p = \sin I/2 \exp(\imath\Omega)$, in which we retain the two dominant terms: the proper term with frequency s and the forced terms with frequency s_6 (see, e.g., Vokrouhlický et al. 2006). In the case of binaries on high-inclination heliocentric orbits, such as those in the Hungaria- or Phocaea-groups, it is necessary to include also additional forced terms due to the terrestrial planets such as s_3 and s_4, because they are more important than the s_6 term and their frequencies are close to s (e.g., Milani et al. 2010). All these harmonic terms were obtained by numerically integrating the heliocentric orbit of the binary over 10 My time interval, and Fourier analysing of the osculating $\zeta = q + \imath p$ values.

With these assumptions, the relative vector $\mathbf{r}$ satisfies

$$\begin{aligned} \frac{d^2\mathbf{r}}{dt^2} + G\,\frac{m_1+m_2}{r^3}\,\mathbf{r} \;&=\; Gm_0\left[\left(\frac{1}{\Delta_{20}^3}-\frac{1}{\Delta_{10}^3}\right)\mathbf{R} - \left(\frac{X_1}{\Delta_{20}^3}+\frac{X_2}{\Delta_{10}^3}\right)\mathbf{r}\right] \\ &+\frac{3\,G\,(m_1+m_2)}{2\,r^5}\left(\frac{R_1}{r}\right)^2 J_2\left\{\left[5\,(\mathbf{r}\cdot\mathbf{s})^2 - r^2\right]\mathbf{r} - 2r^2\,(\mathbf{r}\cdot\mathbf{s})\,\mathbf{s}\right\} \;, \end{aligned} \tag{A.1}$$

where m_0 is the solar mass, $\Delta_{10}^2 = R^2 + 2\,X_2\,(\mathbf{r}\cdot\mathbf{R}) + X_2^2 r^2$ and $\Delta_{20}^2 = R^2 - 2\,X_1\,(\mathbf{r}\cdot\mathbf{R}) + X_1^2 r^2$ are mutual distances of the primary and the secondary components in the binary to the Sun, and $\mathbf{s}$ is the direction of the spin vector of primary. The latter evolves due to gravitational torques exerted by the satellite and the Sun, and we have

$$\frac{d\mathbf{s}}{dt} = \frac{3\,Gm_2}{r^5\omega}\frac{C-A}{C}\,(\mathbf{r}\cdot\mathbf{s})\,(\mathbf{r}\times\mathbf{s}) + \frac{3\,Gm_0}{R^5\omega}\frac{C-A}{C}\,(\mathbf{R}\cdot\mathbf{s})\,(\mathbf{R}\times\mathbf{s}) \;, \tag{A.2}$$

where ω is the angular rotation frequency of the primary (constant in our model). Here, the first term is the satellite's torque and the second term is the Sun's torque. Because $r \ll R$, the satellite's term "nominally dominates", but if the satellite is very close to the primary's equator the solar term also contributes. Obviously, for a spherical primary ($\gamma = 1$ and thus $(C-A)/C = 0$) the spin $\mathbf{s}$ is fixed and the relative orbit of the binary evolves as in the point-mass problem.

Equations (A.1) and (A.2) are numerically propagated using a Burlish-Stoer scheme with variable timestep complying to a chosen accuracy level (e.g., Press et al. 2007). Therefore, our characteristic timestep is typically a fraction of hour. The initial data for $(\mathbf{r}, d\mathbf{r}/dt, \mathbf{s})$ correspond to a near-circular orbit in the equatorial plane of the primary (thus $\mathbf{s} \parallel \mathbf{r}\times d\mathbf{r}/dt$; for sake of simplicity we did not explore solutions with the satellite orbit inclined to the primary's equator). Its semimajor axis $a_{\rm orb}$ is determined by the observed orbital period $P_{\rm orb}$ in Table 1. The initial orientation of the primary spin axis $\mathbf{s}$ is either determined by the orbital pole from Table 1, or we run a sample of simulations with several initial latitudes in order to test short-term stability of the solution: $B_{\rm p} = 0°$, $B_{\rm p} = \pm 20°$, $B_{\rm p} = \pm 40°$, $B_{\rm p} = \pm 60°$ and $B_{\rm p} = \pm 80°$. We still have to select the initial ecliptic longitude $L_{\rm p}$ of $\mathbf{s}$: given the possible circulation of $\mathbf{s}$ about

the Cassini states related to the precessing orbit, we choose $L_{\rm p,1} = \Omega + 90^\circ$ and $L_{\rm p,2} = \Omega + 270^\circ$. Intermediate values of $L_{\rm p}$ would lead to solutions that are represented as a composition of the chosen cases. For definiteness, we choose the primary geometrical oblateness $\gamma = 0.89$, which is the value determined for the best studied binary case of (66391) 1999 KW4 (Ostro et al. 2006); however, our results and conclusions are not overly sensitive to this value. Our model is only adequate to describe the binary evolution over a moderate timescale, but is fundamentally incomplete to represent a long-term evolution. For that reason we set the maximum time of integration to 500 ky. Obviously, we also stop the simulation when the distance r of the primary and secondary components would become: (i) smaller than sum of their radii (estimated in Table 1), or (ii) larger than the estimated Hill radius of their gravitational interaction (typically few hundreds of primary radii).

As demonstrated in Sec. 6, the oblateness of the primary efficiently couples the evolution of its spin axis $\mathbf{s}$ and the binary orbital angular momentum $(m_1 + m_2)\, X_1 X_2\, \mathbf{r} \times (d\mathbf{r}/dt)$ for compact systems (i.e., when $r \ll d_2$). In this situation, the orbit pole evolution may be obtained by numerical integration of a much simpler system

$$\frac{d\mathbf{s}'}{dt} = -\left[\alpha_{\rm eff}\,(\mathbf{n}\cdot\mathbf{s}')\,\mathbf{n} + \boldsymbol{\sigma}\right] \times \mathbf{s}' \,, \tag{A.3}$$

where $\mathbf{s}'$ is the primary and orbit pole referred to the system of axes precessing with the binary's heliocentric orbit, such that the x-axis is rotated in the osculating plane by $-\Omega$ from the ascending node and the z-axis is along the osculating normal $\mathbf{n}$ to the heliocentric orbital plane, $\alpha_{\rm eff}$ is the effective precession constant from Eq. (10) and $\boldsymbol{\sigma} = (\sigma_1, \sigma_2, \sigma_3)^T$, with

$$\sigma_1 = \cos\Omega\,(dI/dt) - \sin I \sin\Omega\;(d\Omega/dt) \,, \tag{A.4}$$
$$\sigma_2 = \sin\Omega\,(dI/dt) + \sin I \cos\Omega\;(d\Omega/dt) \,, \tag{A.5}$$
$$\sigma_3 = \sin^2 I/2\,(d\Omega/dt) \,. \tag{A.6}$$

Here, I and Ω are the osculating values of inclination and longitude of ascending node of the binary heliocentric orbit, and dI/dt and $d\Omega/dt$ are their rates induced by planetary perturbations. Not only the system (A.3) is much simpler than Eqs. (A.1) and (A.2), but most importantly it eliminates orbital motion of the binary. As a result, the shortest timescale involved is that of secular evolution of the binary's heliocentric orbit and consequently one can take a much longer integration timestep. Additionally, an efficient Lie-Poisson integration scheme is available for this system (e.g., Breiter et al. 2005), which optimizes the integrator speed. Therefore a sample of binary's orbit-pole evolution can be efficiently obtained by integration of (A.3). The scheme may even contain a slow, adiabatic, evolution of the binary orbit induced by tides or BYORP effects (e.g., Taylor and Margot 2010, 2011, Ćuk and Burns 2004, Ćuk and Nesvorný 2010, McMahon and Scheeres 2010). In this case the precession constant $\alpha_{\rm eff}$ would slowly evolve, reflecting slow changes in the satellite orbit.

References

Benner, L.A.M., Margot, J., Nolan, M.C., Giorgini, J.D., Brozovic, M., Scheeres, D.J., Magri, C., Ostro, S.J., 2010. Radar imaging and a physical model of binary asteroid 65803 Didymos. Bull. Am. Astron. Soc. 42, 1056.

Bertotti, B., Farinella, P., Vokrouhlický, D., 2003. Physics of the Solar System (Kluwer Academic Publishers, New York).

Bottke, W.F., Vokrouhlický, D., Rubincam, D.P., Nesvorný, D., 2006. The Yarkovsky and YORP effects: Implications for asteroid dynamics. Annu. Rev. Earth Planet. Sci. 34, 157–191.

Bottke, W.F., Durda, D.D., Nesvorný, D., Jedicke, R., Morbidelli, A., Vokrouhlický, D., Levison, H.F., 2005. Linking the collisional history of the main asteroid belt to its dynamical excitation and depletion. Icarus 179, 63–94.

Breiter, S., Nesvorný, D., Vokrouhlický, D., 2005. Efficient Lie-Poisson integrator for secular spin dynamics of rigid bodies. Astron. J. 130, 1267–1277.

Carruba, V., Burns, J.A., Nicholson, P.D., Gladman, B.J., 2002. On the inclination distribution of the Jovian irregular satellites. Icarus 158, 434–449.

Colombo, G., 1966. Cassini's second and third laws. Astron. J. 71, 891–896.

Čapek, D., Vokrouhlický, D., 2004. The YORP effect with finite thermal conductivity. Icarus 172, 526–536.

Ćuk, M., Burns, J.A., 2004. Effects of thermal radiation on the dynamics of binary NBAs. Icarus 176, 418–431.

Ćuk, M., Nesvorný, D., 2010. Orbital evolution of small binary asteroids. Icarus 207, 732–743.

French, R.G., and 17 colleagues, 1993. Geometry of the Saturn system from the 3 July 1989 occultation of 28 Sgr and Voyager observations. Icarus 103, 163–214.

Goldreich, P., 1965. Inclination of satellite orbits about an oblate precessing planet. Astron. J. 70, 5–9.

Hanuš, J., and 14 colleagues, 2011. A study of asteroid pole-latitude distribution based on an extended set of shape models derived by the lightcurve inversion method. Astron. Astrophys. 530, A134.

Henrard, J., Murigande, C., 1987. Colombo's top. Celest. Mech. 40, 345–366.

Kaasalainen, M., Torppa, J., Muinonen, K., 2002. Models of twenty asteroids from photometric data. Icarus 159, 369–395.

Kozai, Y., 1962. Secular perturbations of asteroids with high inclination and

eccentricity. Astron. J. 67, 591–598.

McMahon, J., Scheeres, D.J., 2010. Detailed prediction for the BYORP effect on binary near-Earth Asteroid (66391) 1999 KW4 and implications for the binary population. Icarus 209, 494–509.

Mignard, F., 1981. Evolution of the Martian satellites. Mon. Not. Roy. Astron. Soc. 194, 365–379.

Milani, A., Knežević, Z., Novaković, B., Cellino, A., 2010. Dynamics of the Hungaria asteroids. Icarus 207, 769–794.

Murray, C.D., Dermott, S.F., 1999. Solar System Dynamics. Cambridge University Press

Nesvorný, D., Alvarellos, J.L.A., Dones, L., Levison, H.F., 2003. Orbital and collisional evolution of the irregular satellites. Astron. J. 126, 398–429.

Ostro, S.J., and 15 colleagues, 2006. Radar imaging of binary near-Earth asteroid (66391) 1999 KW4. Science 314, 1276–1280.

Pravec, P., and 56 colleagues, 2006. Photometric survey of binary near-Earth asteroids. Icarus 181, 63–93.

Pravec, P., Harris, A.W., 2007. Binary asteroid population. 1. Angular momentum content. Icarus 190, 250–259.

Press, W.H., Teukolsky, S.A., Vetterling, W.T., Flannery, B.P., 2007. Numerical Recipes (Cambridge University Press, Cambridge)

Scheeres, D.J., 2007. Rotational fission of contact binary asteroids. Icarus 189, 370–385.

Scheirich, P., Pravec, P., 2009. Modeling of lightcurves of binary asteroids. Icarus 200, 531–547.

Shepard, M.K., and 12 colleagues, 2006. Radar and infrared observations of binary near-Earth asteroid 2002 CE26. Icarus 184, 198–210.

Stephens, R.D., Warner, B.D., Harris, A.W., 2010. A proposed standard for reporting asteroid lightcurve data. Bull. Amer. Astron. Soc. 42, 1035.

Taylor, P.A., Margot, J.-L., 2010. Tidal evolution of close binary asteroid systems. Celest. Mech. Dyn. Astr. 108, 315–338.

Taylor, P.A., Margot, J.-L., 2011. Binary asteroid systems: Tidal end states and estimates of material properties. Icarus 212, 661–676.

Taylor, P.A., Margot, J.-L., Nolan, M.C., Benner, L.A.M., Ostro, S.J., Giorgini, J.D., Magri, C., 2008. The shape, mutual orbit, and tidal evolution of binary near-Earth asteroid 2004 DC. LPIC 1405, 8322.

Vokrouhlický, D., Nesvorný, D., Bottke, W.F., 2006. Secular spin dynamics of inner main-belt asteroids. Icarus 184, 1–28.

Walsh, K.J., Richardson, D.C., Michel, P., 2008. Rotational breakup as the origin of small binary asteroids. Nature 454, 188–191.

Ward, W.R., 1975. Tidal friction and generalized Cassini's laws in the solar system. Astron. J. 80, 64–70.

Warner, B.D., Harris, A.W., Pravec, P., 2009a. An analysis of slow rotators among the Hungaria asteroids. Bull. Amer. Astron. Soc. 41, XX.

Warner, B.D., Harris, A.W., Vokrouhlický, D., Nesvorný, D., Bottke, W.F., 2009b. Analysis of the Hungaria asteroid population. Icarus 204, 172–182.

Table 1
Parameters of 18 binary asteroids observed in more than one apparition

Binary system	D_1(km)	D_2/D_1	P_1(h)	$P_{\rm orb}$(h)	P_2(h)	$a_{\rm orb}/D_1$	$L_{\rm p}$ (°)	$B_{\rm p}$ (°)	ϵ (°)	$a_{\rm h}$(AU)	$i_{\rm h}$(°)
(1338) Duponta	7.4	0.24	3.85453	17.5680	(17.57)	2.0	0 - 360	+66 - +90	0 - 21	2.264	4.82
(1453) Fennia	7.0	0.28	4.4121	23.00351		2.6	89 - 118	−70 - −62	172 - 180	1.897	23.68
(1830) Pogson	7.8	(0.30)	2.57003	24.24580		(2.5)	130 - 274	−86 - −74	162 - 180	2.188	3.95
(2006) Polonskaya	5.5	(0.23)	3.1180	19.153		(2.1)				2.325	4.92
(2044) Wirt	5.6	0.25	3.6897	18.976	(18.97)	2.1	349 - 23	−72 - −52	120 - 143[a]	2.380	23.98
(2 pole solutions)				18.965			168 - 203	+58 - +72	37 - 53		
(2577) Litva	4.0	(0.34)	2.81292	35.8723		(3.2)	253 - 348	−84 - −68	158 - 178	1.904	22.91
(2754) Efimov	4.9	0.22	2.44967	14.77578		1.8	0 - 360	−90 - −66	154 - 180	2.228	5.71
(3309) Brorfelde	4.7	0.26	2.5042	18.46444	18.45	2.0	116 - 154	−74 - −64	168 - 180	1.817	21.14
(3868) Mendoza	8.3	0.17	2.77089	12.195		1.5				2.333	8.10
(4029) Bridges	7.7	0.27	3.5750	16.31701		1.9	0 - 360	−90 - −62	157 - 180	2.525	5.44
(5477) Holmes	2.9	0.39	2.9941	24.4036	(24.41)	2.5	320 - 332	+38 - +64[b]	5 - 30[b]	1.917	22.55
(5905) Johnson	3.6	0.38	3.7823	21.75639		2.3	30 - 58	+60 - +76	0 - 14	1.910	27.52
(2 pole solutions)				21.79699			210 - 254	−56 - −76	167 - 180		
(6084) Bascom	5.8	0.37	2.7453	43.51	(43.5)	3.7	267 - 378	−76 - −56	127 - 169	2.313	23.01
(6244) Okamoto	4.4	0.25	2.8957	20.3105		2.2	0 - 360	+54 - +90[c]	0 - 33[c]	2.160	5.40
(2 pole solutions)				20.3232			0 - 360	−90 - −58[d]	151 - 180[d]		
(6265) 1985 TW3	5.2	(0.32)	2.7092	15.86		1.9				2.166	4.11
(9617) Grahamchapman	2.8	(0.27)	2.28561	19.3817		2.1	0 - 360	+48 - +90[e]	0 - 38[e]	2.224	6.14
(2 pole solutions)				19.3915			0 - 360	−90 - −50[f]	141 - 180[f]		
(17260) 2000 JQ58	3.2	0.26	3.1287	14.7577	14.745	1.8	0 - 360	−90 - −56[g]	147 - 180[g]	2.204	5.28
(2 pole solutions)				14.7523			0 - 360	+46 - +90[h]	0 - 43[h]		
(76818) 2000 RG79	2.8	(0.35)	3.1665	14.11960	14.127	1.7	28 - 360	+72 - +90	0 - 22	1.930	18.13
(2 pole solutions)				14.12998			0 - 360	−90 - −70	158 - 180		

Values in parentheses have following meanings: the estimated size ratios D_2/D_1 may be only lower limits, as the assumption of that we observed total events or that a possible third component has a negligible size may not hold; the secondary period (P_2) solutions are likely but not entirely unique; and the estimates of the relative semi-major axis $a_{\rm orb}/D_1$ may be affected by presence of the possible third component. See the electronic files available at http://www.asu.cas.cz/∼asteroid/binastdata.htm for references, comments, additional estimated parameters, and uncertainties.

[a] Quality of the fit decreases with decresing ϵ, so the higher values are preferred.

[b] Model bulk density increases from 0.8 to 1.9 g cm^{-3} with increasing $B_{\rm p}$. The most plausible solution is for $B_{\rm p} \sim +60°$ and $\varepsilon \sim 8°$

[c] For model bulk density > 1.0 g cm^{-3} the values of $B_{\rm p}$ and ϵ are constrained to be $> +64°$ and $< 21°$, respectively.

[d] For model bulk density > 1.0 g cm^{-3} the values of $B_{\rm p}$ and ϵ are constrained to be $< -66°$ and $> 159°$, respectively.

[e] For model bulk density > 1.0 g cm^{-3} the values of $B_{\rm p}$ and ϵ are constrained to be $> +62°$ and $< 24°$, respectively.

[f] For model bulk density > 1.0 g cm^{-3} the values of $B_{\rm p}$ and ϵ are constrained to be $< -62°$ and $> 156°$, respectively.

[g] For model bulk density > 1.0 g cm^{-3} the values of $B_{\rm p}$ and ϵ are constrained to be $< -62°$ and $> 153°$, respectively.

[h] For model bulk density > 1.0 g cm^{-3} the values of $B_{\rm p}$ and ϵ are constrained to be $> +62°$ and $< 27°$, respectively.

Table 2
Epochs of mutual events in return binaries

Binary system	Date (UT)	$L(^\circ)$	$B(^\circ)$	$L_{\rm h}(^\circ)$	$B_{\rm h}(^\circ)$	EventDet
(1338) Duponta	2007-03-06.9	160.1	-2.5	162.7	-1.4	P
(1338) Duponta	2010-01-05.0	82.0	7.2	92.7	3.9	P
(1453) Fennia	2007-11-04.4	76.8	33.9	58.7	18.9	P
(1453) Fennia	2009-08-14.6	293.1	-39.5	309.3	-20.4	P
(1830) Pogson	2007-04-18.6	220.6	6.7	214.8	3.6	P
(1830) Pogson	2010-02-20.7	183.7	2.6	169.3	1.5	P
(2006) Polonskaya	2005-11-01.2	46.9	6.8	42.6	3.3	P
(2006) Polonskaya	2008-06-05.3	294.3	-7.7	278.4	-4.9	N
(2044) Wirt	2005-12-05.9	56.5	13.7	66.8	5.7	P
(2044) Wirt	2008-08-24.3	316.7	-35.5	322.3	-24.0	N
(2577) Litva	2009-03-02.2	132.3	-28.2	149.4	-13.0	P
(2577) Litva	2010-08-11.3	335.4	25.6	327.1	13.8	P
(2754) Efimov	2006-08-14.2	0.9	10.6	339.1	5.1	P
(2754) Efimov	2011-01-31.0	139.2	-6.2	135.8	-3.7	P
(3309) Brorfelde	2005-10-25.2	21.1	-2.5	26.7	-1.2	P
(3309) Brorfelde	2009-01-28.3	147.4	39.6	136.7	20.3	P
(3868) Mendoza	2009-04-25.5	221.4	10.0	218.9	6.0	P
(3868) Mendoza	2010-09-07.0	25.2	-3.6	6.9	-2.1	P
(4029) Bridges	2006-04-11.6	222.3	-0.3	213.0	-0.2	P
(4029) Bridges	2007-10-06.0	356.8	4.6	2.5	2.9	P
(5477) Holmes	2005-11-02.3	47.0	-5.3	43.2	-2.5	P
(5477) Holmes	2007-06-10.5	225.7	-10.7	242.7	-5.6	P
(5905) Johnson	2005-04-01.3	185.4	38.8	188.7	20.9	P
(5905) Johnson	2008-05-13.4	279.3	43.6	254.3	25.6	P
(6084) Bascom	2005-12-29.6	139.5	-18.4	120.5	-10.9	P
(6084) Bascom	2008-09-01.6	351.8	-15.2	345.4	-7.5	N
(6244) Okamoto	2006-09-26.2	2.9	6.2	2.9	2.8	P
(6244) Okamoto	2009-08-14.6	320.3	-2.0	321.1	-1.0	P
(6265) 1985 TW3	2007-07-15.5	297.4	-8.8	294.6	-3.9	P
(6265) 1985 TW3	2010-06-13.6	244.8	-4.0	253.7	-2.0	P
(9617) Grahamchapman	2006-01-27.3	139.3	-6.3	133.4	-3.3	P
(9617) Grahamchapman	2008-12-26.2	63.7	-11.3	78.7	-6.1	P
(17260) 2000 JQ58	2006-01-29.6	148.0	-10.0	138.0	-4.7	P
(17260) 2000 JQ58	2009-01-01.3	65.0	-8.8	82.8	-4.7	P
(76818) 2000 RG79	2005-08-07.3	342.2	21.1	327.9	10.8	P
(76818) 2000 RG79	2008-10-03.4	73.3	28.3	41.3	17.2	P

The ecliptic coordinates are in the equinox of J2000. For definition of positive/negative (P/N) event detection, see text.

Table 3
Results of the simulation of the binary survey for assumed isotropic distribution of orbit poles

Binary system	$n_{1\text{stapp}}$	$n_{2\text{ndapp}}$	Probability ($\frac{n_{2\text{ndapp}}}{n_{1\text{stapp}}}$)
(1338) Duponta	7617	1286	0.169
(1453) Fennia	9985	2963	0.297
(1830) Pogson	7152	1749	0.245
(2006) Polonskaya	7492	1406	0.188
(2044) Wirt	8913	2212	0.248
(2577) Litva	8988	6620	0.737
(2754) Efimov	10934	4469	0.409
(3309) Brorfelde	8264	2491	0.301
(3868) Mendoza	8983	3494	0.389
(4029) Bridges	9269	2927	0.316
(5477) Holmes	7565	6091	0.805
(5905) Johnson	10208	3826	0.375
(6084) Bascom	7606	1390	0.183
(6244) Okamoto	7073	1567	0.222
(6265) 1985 TW3	9001	2631	0.292
(9617) Grahamchapman	8156	1644	0.202
(17260) 2000 JQ58	10014	2201	0.220
(76818) 2000 RG79	12519	3814	0.305

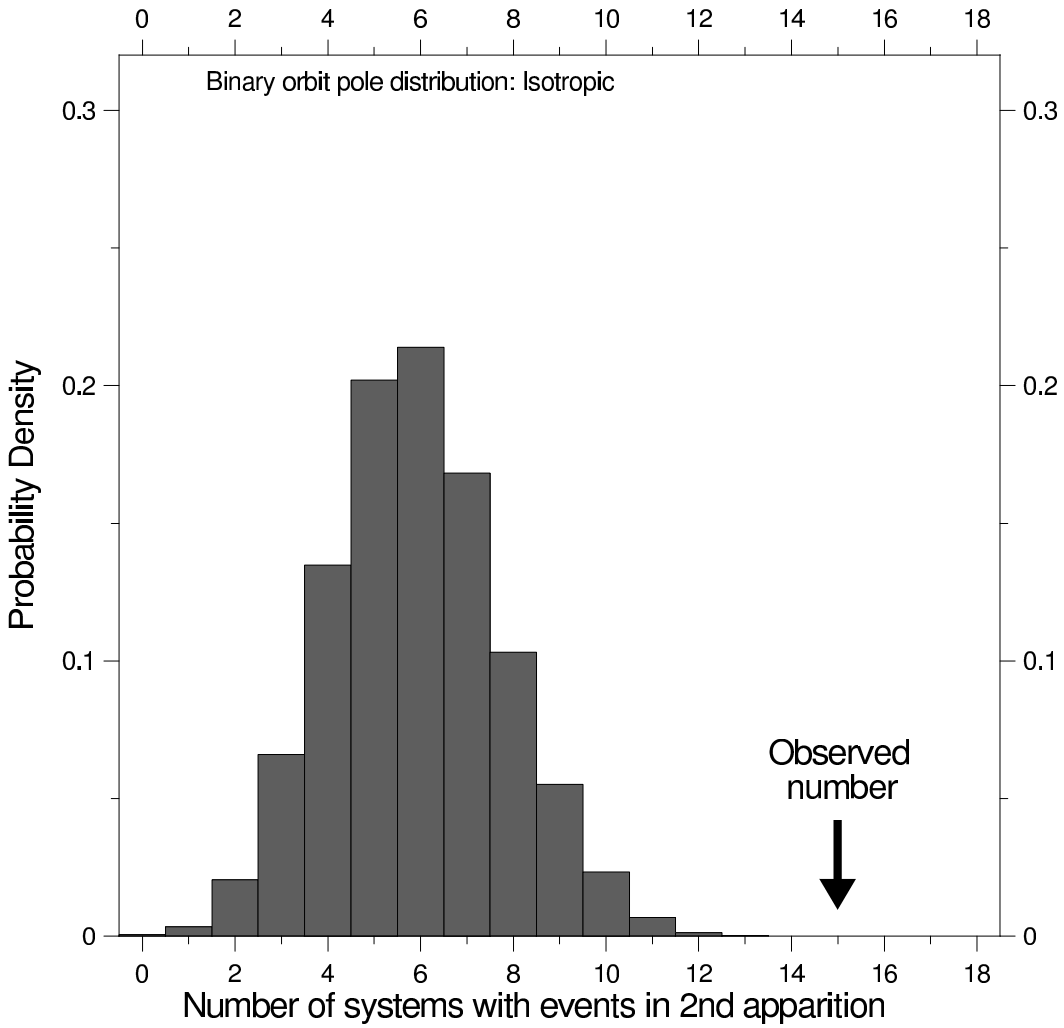

Fig. 1. Estimated probability density of occurence of mutual events in the return apparition in $N_{2\mathrm{app}}$ of the 18 binary systems, assuming an isotropic distribution of orbit poles of binary systems. The observed number (15) is much greater than the prediction for the null hypothesis.

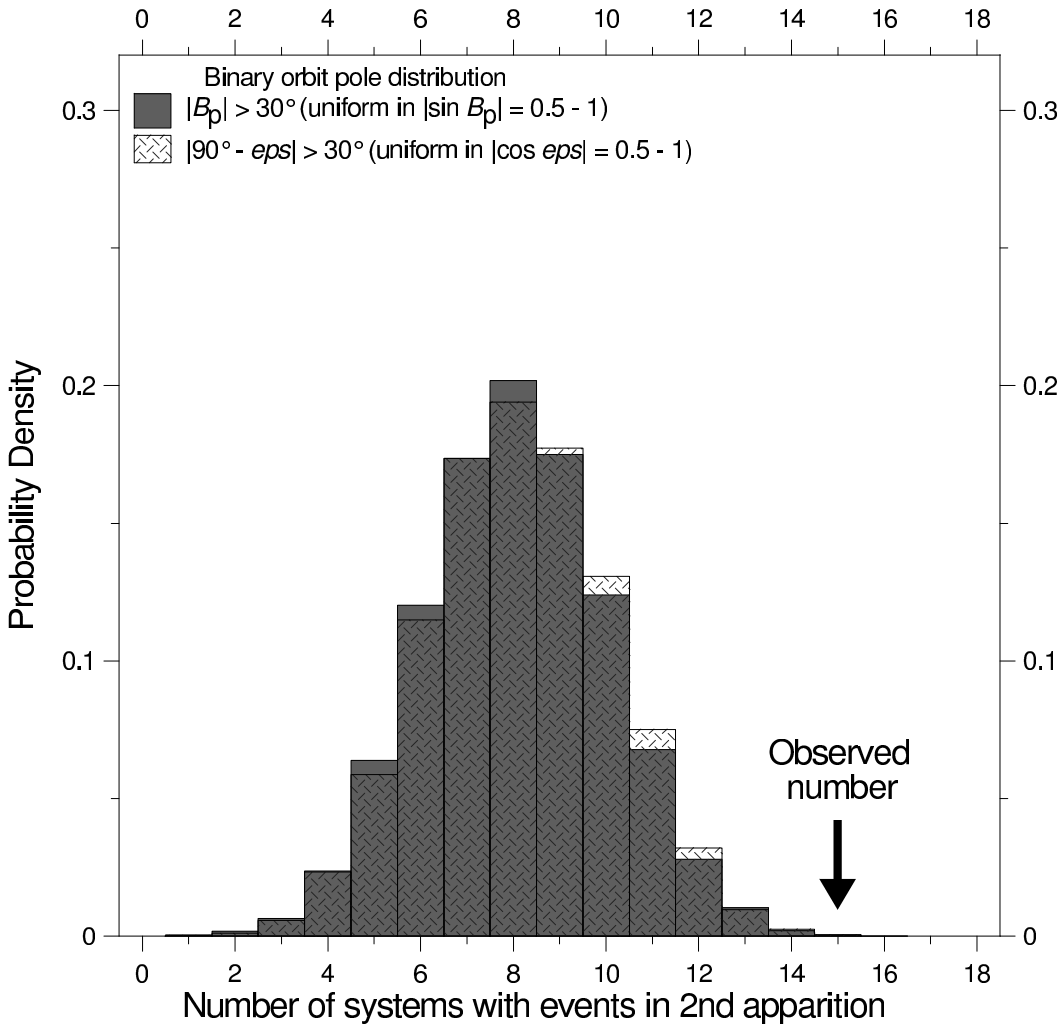

Fig. 2. Estimated probability densities of occurence of mutual events in the return apparition in $N_{2\mathrm{app}}$ of the 18 binary systems, assuming an uniform distribution of orbit poles of binary systems in $|\sin B_\mathrm{p}|$ (filled bins) and $|\cos\epsilon|$ (hatched bins) from $\sin 30^\circ$ to 1.

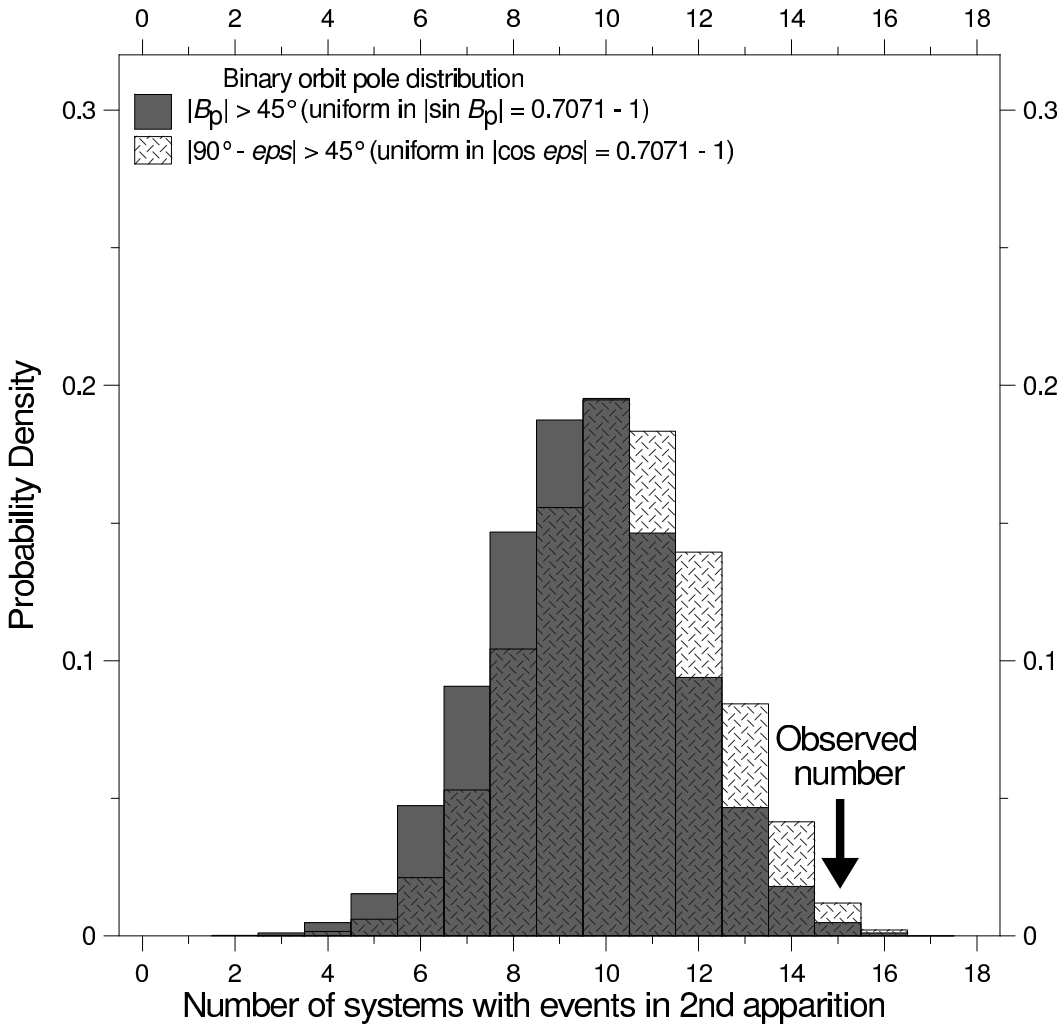

Fig. 3. Estimated probability densities of occurence of mutual events in the return apparition in $N_{2\mathrm{app}}$ of the 18 binary systems, assuming an uniform distribution of orbit poles of binary systems in $|\sin B_\mathrm{p}|$ (filled bins) and $|\cos \epsilon|$ (hatched bins) from $\sin 45^\circ$ to 1.

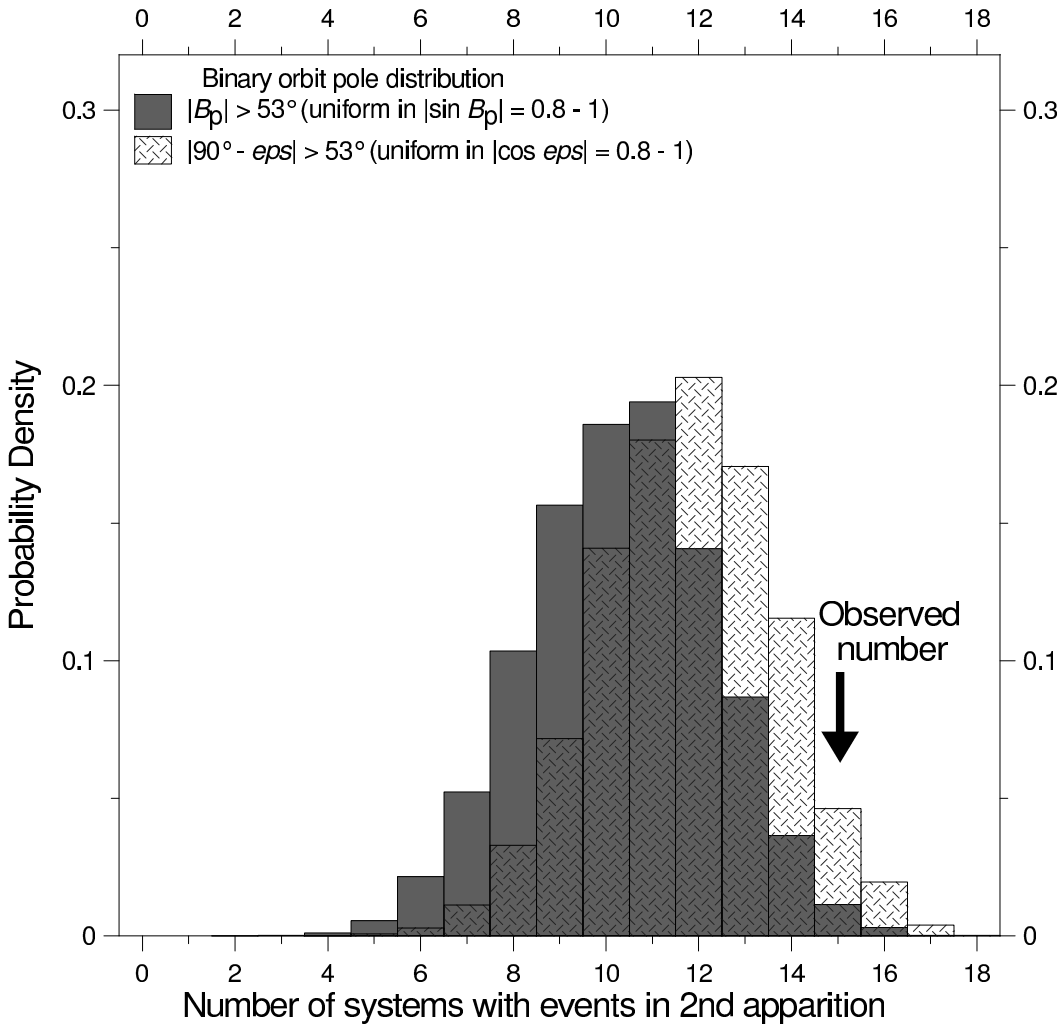

Fig. 4. Estimated probability densities of occurence of mutual events in the return apparition in $N_{2\mathrm{app}}$ of the 18 binary systems, assuming an uniform distribution of orbit poles of binary systems in $|\sin B_\mathrm{p}|$ (filled bins) and $|\cos\epsilon|$ (hatched bins) from $\sin 53^\circ$ to 1.

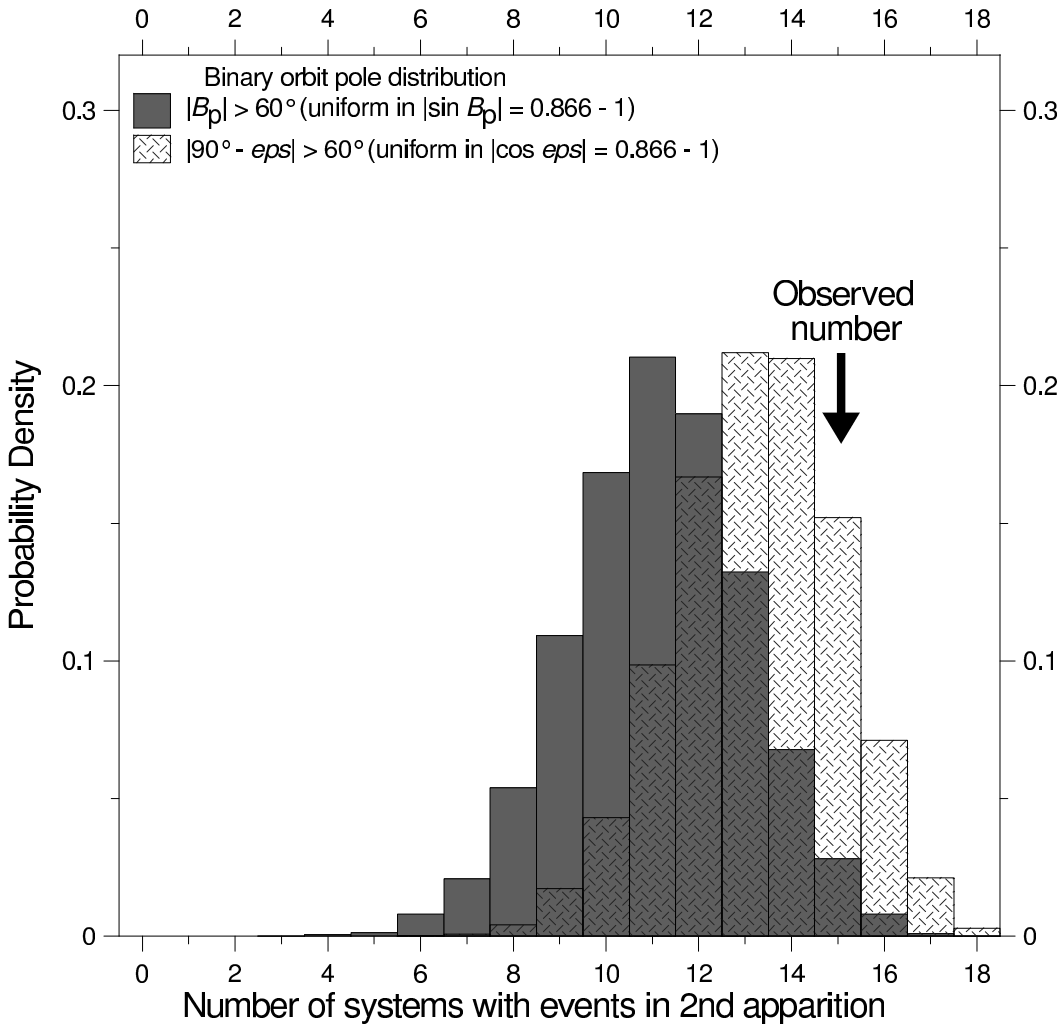

Fig. 5. Estimated probability densities of occurence of mutual events in the return apparition in $N_{2\mathrm{app}}$ of the 18 binary systems, assuming an uniform distribution of orbit poles of binary systems in $|\sin B_{\mathrm{p}}|$ (filled bins) and $|\cos \epsilon|$ (hatched bins) from $\sin 60^{\circ}$ to 1.

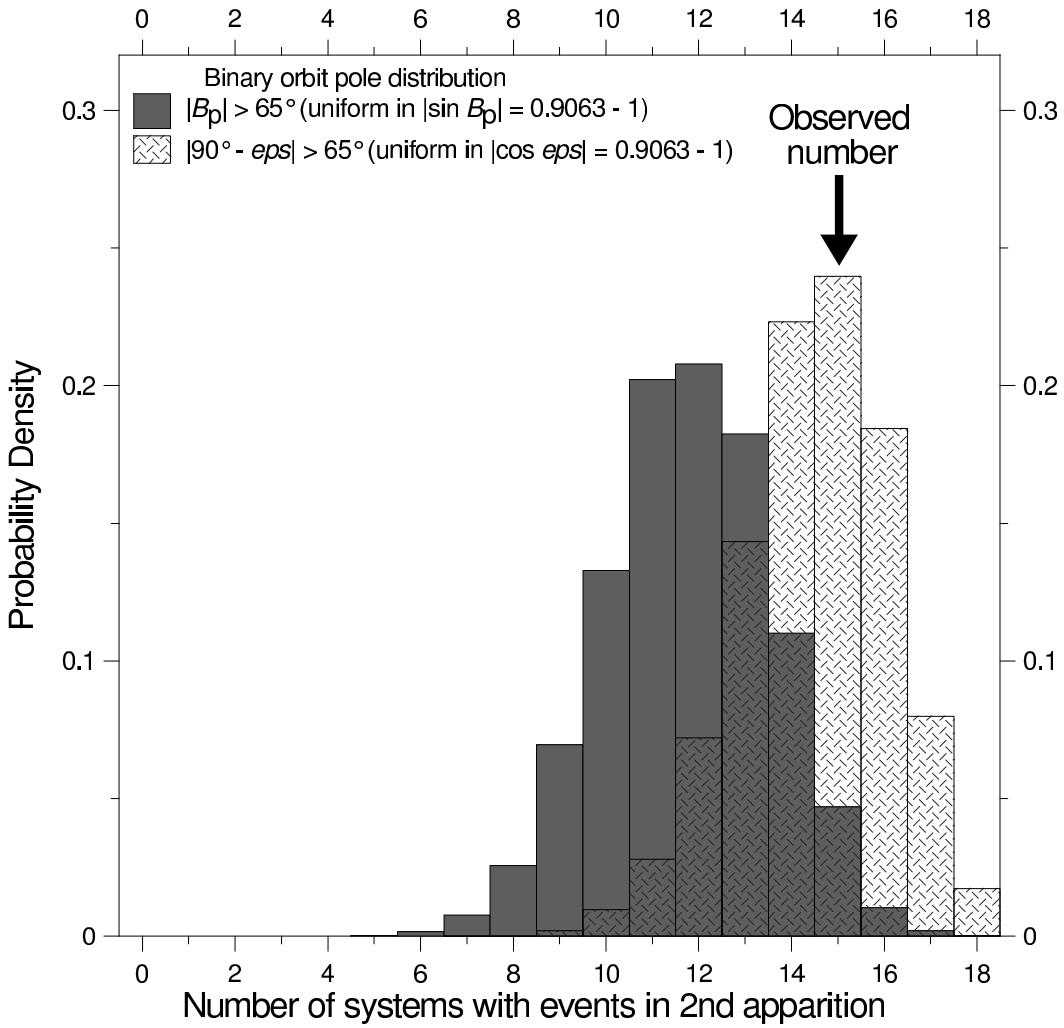

Fig. 6. Estimated probability densities of occurence of mutual events in the return apparition in $N_{2\mathrm{app}}$ of the 18 binary systems, assuming an uniform distribution of orbit poles of binary systems in $|\sin B_{\mathrm{p}}|$ (filled bins) and $|\cos \epsilon|$ (hatched bins) from $\sin 65^\circ$ to 1.

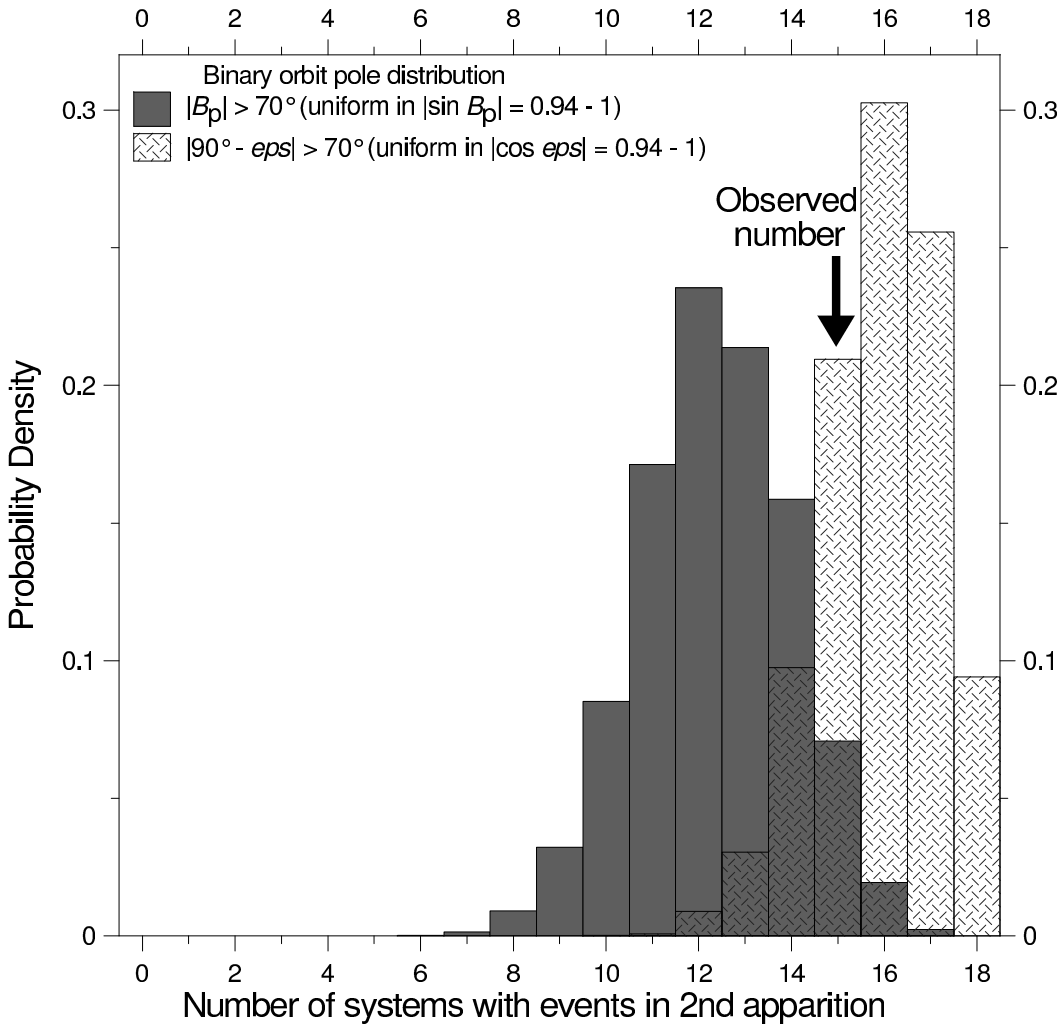

Fig. 7. Estimated probability densities of occurence of mutual events in the return apparition in $N_{2\mathrm{app}}$ of the 18 binary systems, assuming an uniform distribution of orbit poles of binary systems in $|\sin B_{\mathrm{p}}|$ (filled bins) and $|\cos \epsilon|$ (hatched bins) from $\sin 70^{\circ}$ to 1.

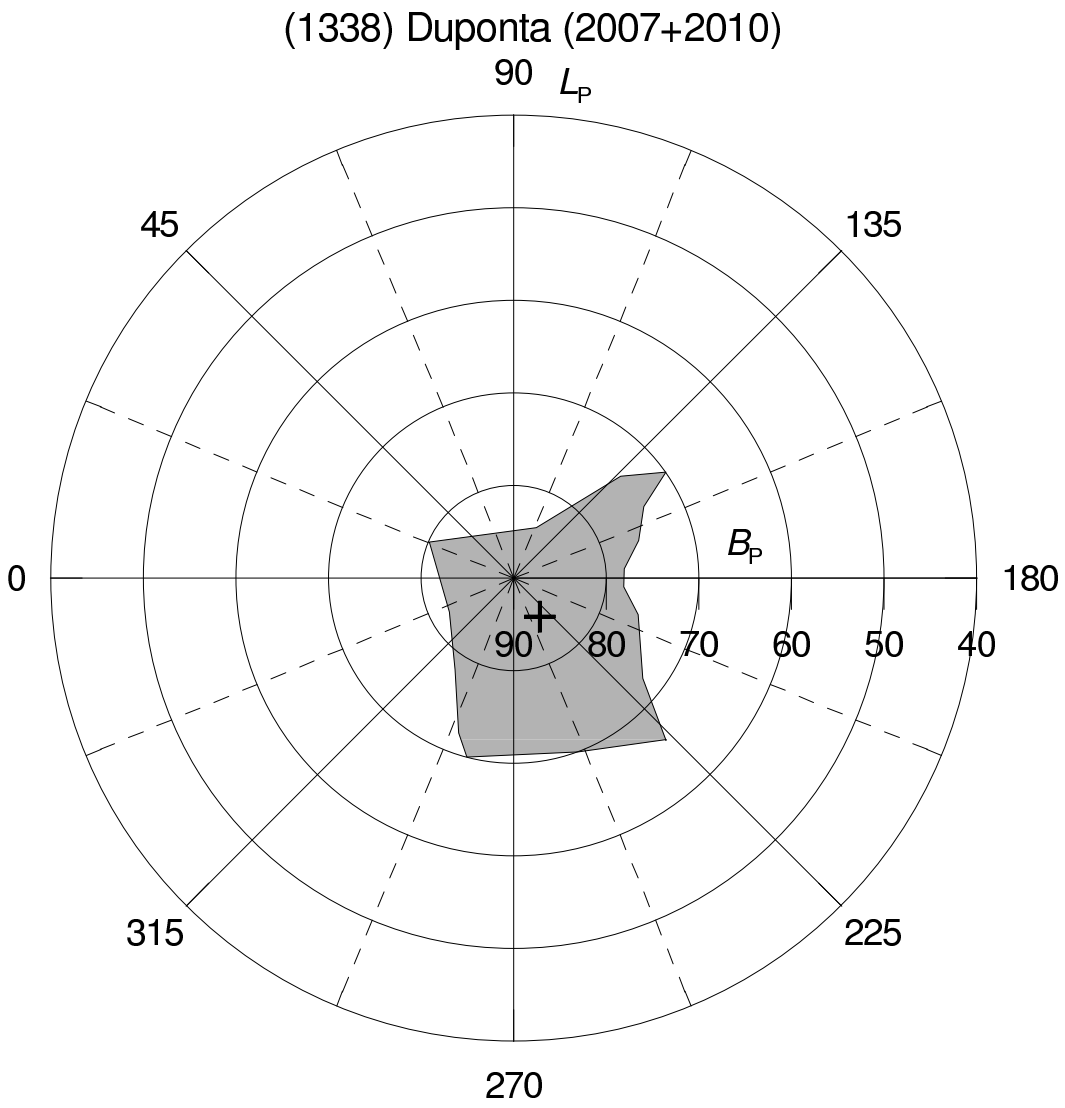

Fig. 8. Area of admissible poles for the mutual orbit of (1338) Duponta in ecliptic coordinates. The north pole of the current asteroid's heliocentric orbit is marked with the cross.

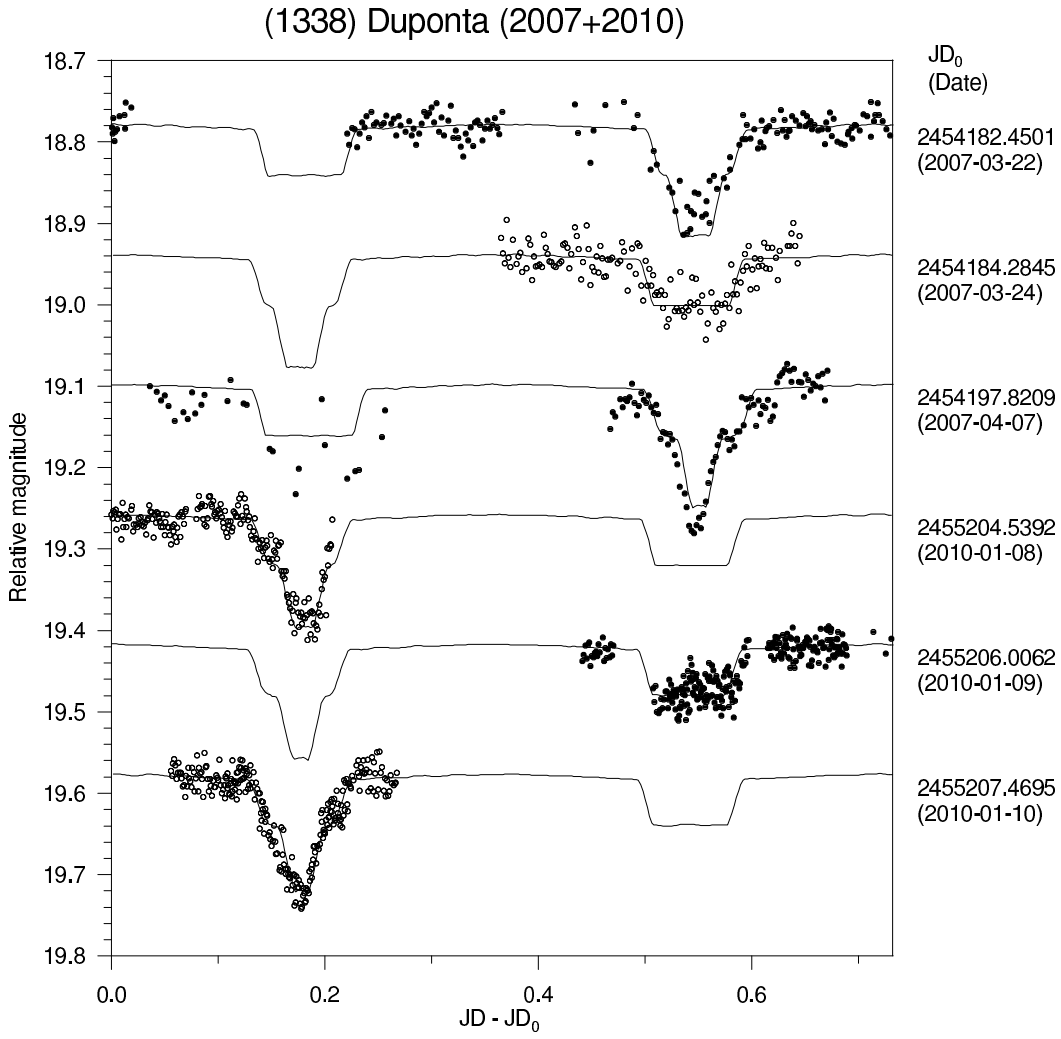

Fig. 9. Sample of the orbital lightcurve component's data of (1338) Duponta in apparitions 2007 and 2010. The observational data (points) are plotted together with the synthetic lightcurve for the best-fit solution (curve). The data sets from different dates are vertically offset for clarity, and different symbols are used for them to avoid confusion. The offsets in date (JD_0) are listed in the right column for each curve. On the first and third curves from the top, the minima are shown in an order opposite (i.e., first the secondary and then the primary event) to the other curves.

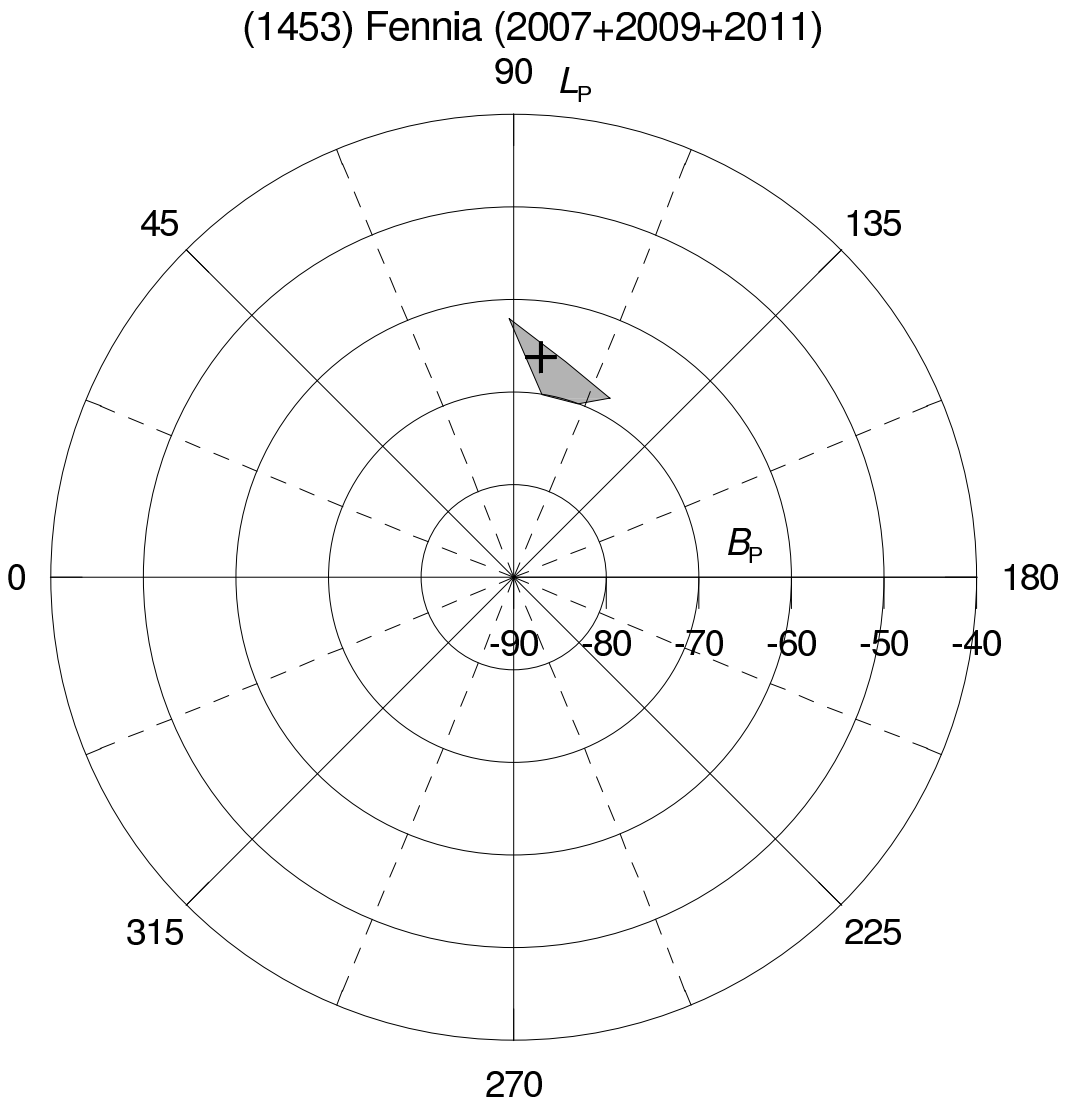

Fig. 10. Area of admissible poles for the mutual orbit of (1453) Fennia in ecliptic coordinates. The south pole of the current asteroid's heliocentric orbit is marked with the cross.

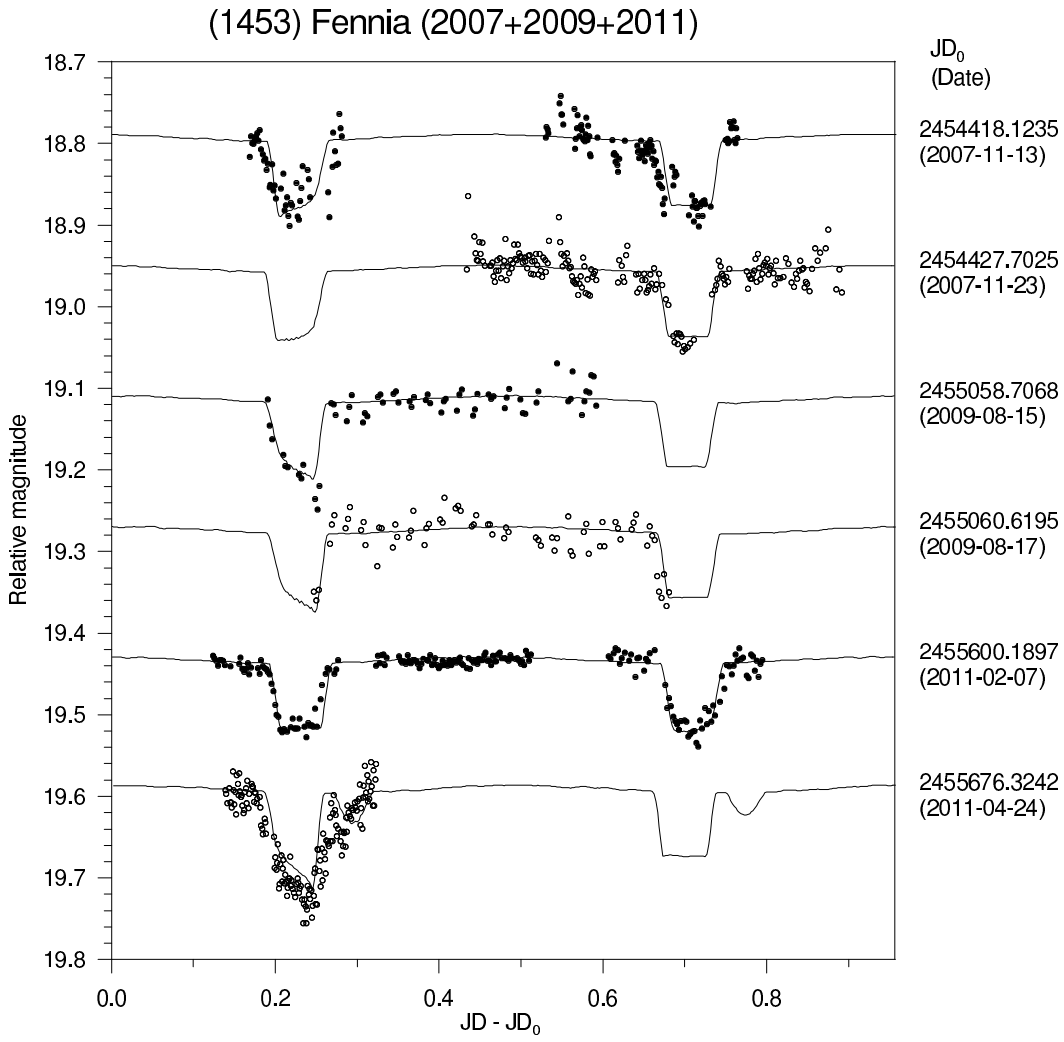

Fig. 11. Sample of the orbital lightcurve component's data of (1453) Fennia in apparitions 2007, 2009, and 2011. The observational data (points) are plotted together with the synthetic lightcurve for the best-fit solution (curve). The data sets from different dates are vertically offset for clarity, and different symbols are used for them to avoid confusion. The offsets in date (JD_0) are listed in the right column for each curve. On the fifth curve from the top, the minima are shown in an order opposite (i.e., first the secondary and then the primary event) to the other curves.

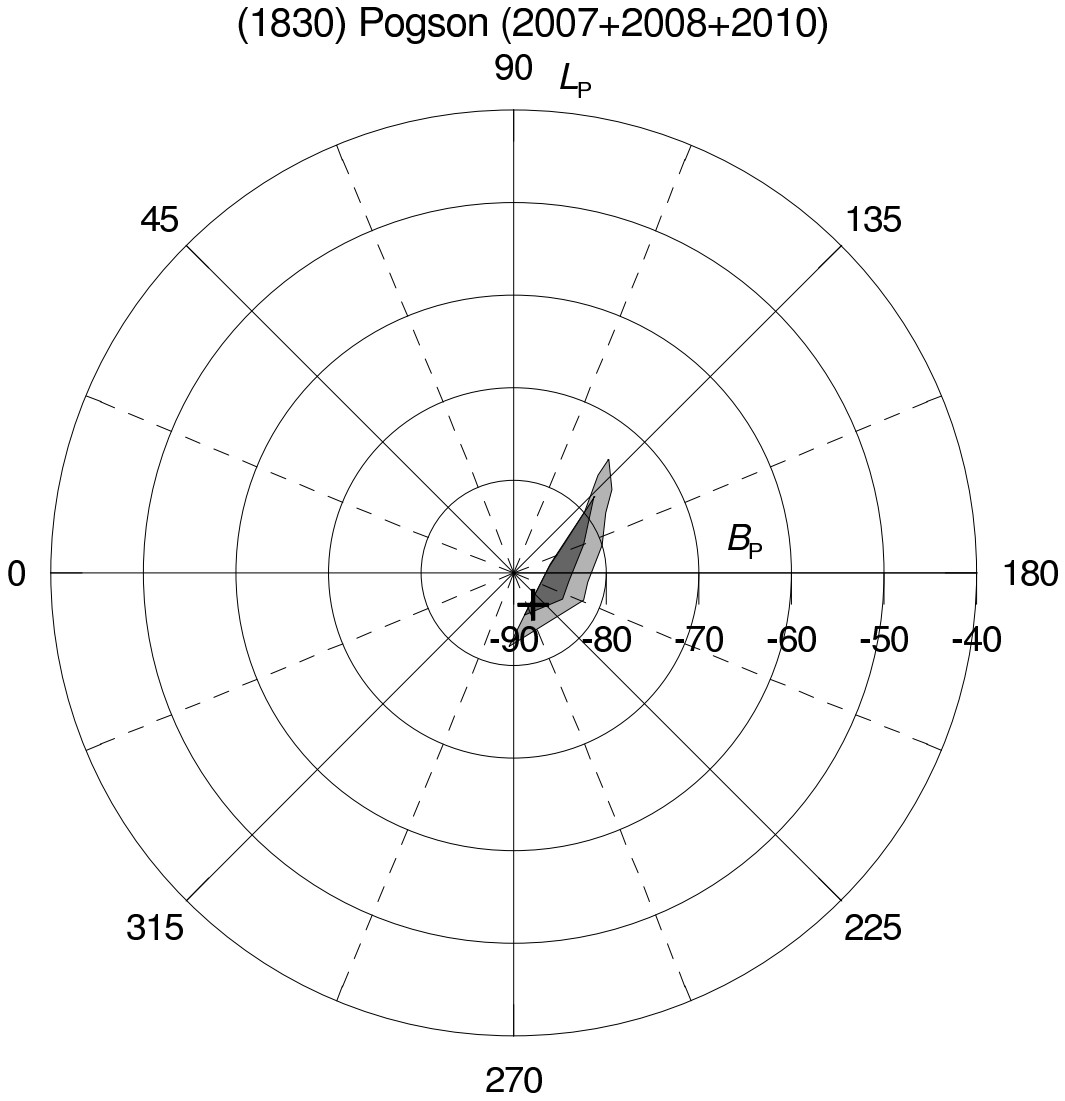

Fig. 12. Area of admissible poles for the mutual orbit of (1830) Pogson in ecliptic coordinates. The solid curve inside the area bounds the admissible poles constrained using the effective diameter of the third body set equal to the effective diameter of the primary. The south pole of the current asteroid's heliocentric orbit is marked with the cross.

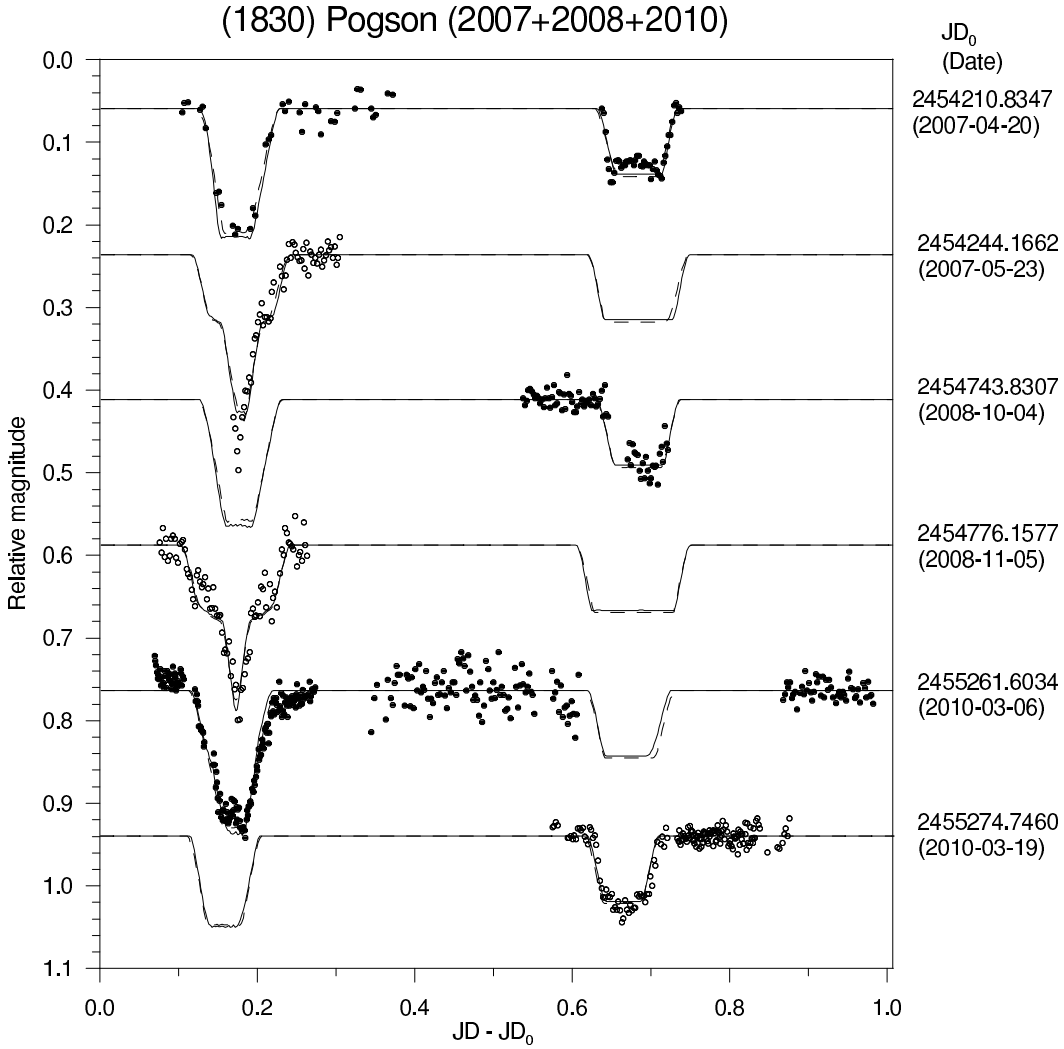

Fig. 13. Sample of the orbital lightcurve component's data of (1830) Pogson in apparitions 2007, 2008, and 2010. The observational data (points) are plotted together with the synthetic lightcurve for the best-fit solution without the third body (solid curve) and with the third body with diameter equal to D_1 (dashed curve). The data sets from different dates are vertically offset for clarity, and different symbols are used for them to avoid confusion. The offsets in date (JD_0) are listed in the right column for each curve.

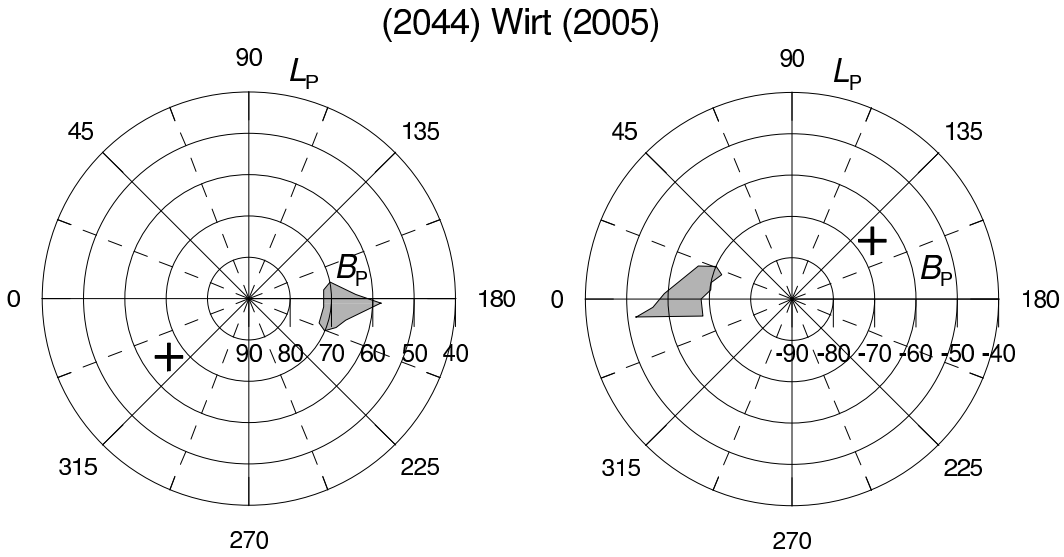

Fig. 14. Area of admissible poles for the mutual orbit of (2044) Wirt in ecliptic coordinates. The north and the south pole of the current asteroid's heliocentric orbit are marked with the crosses.

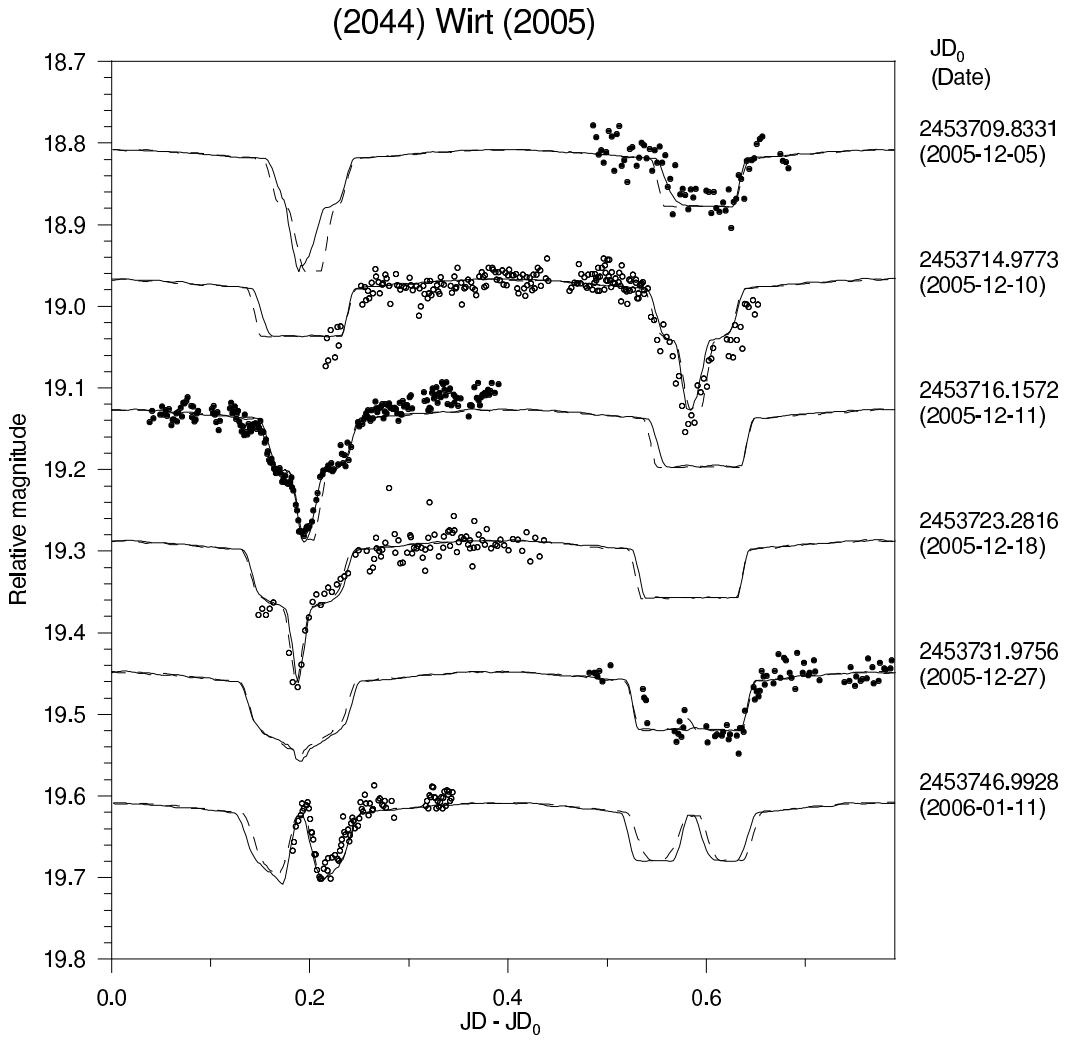

Fig. 15. Sample of the orbital lightcurve component's data of (2044) Wirt in apparition 2005. The observational data (points) are plotted together with the synthetic lightcurves for the two best-fit solutions (retrograde – solid curve, prograde – dashed curve). The data sets from different dates are vertically offset for clarity, and different symbols are used for them to avoid confusion. The offsets in date (JD_0) are listed in the right column for each curve. On the second curve from the top, the minima are shown in an order opposite (i.e., first the secondary and then the primary event) to the other curves.

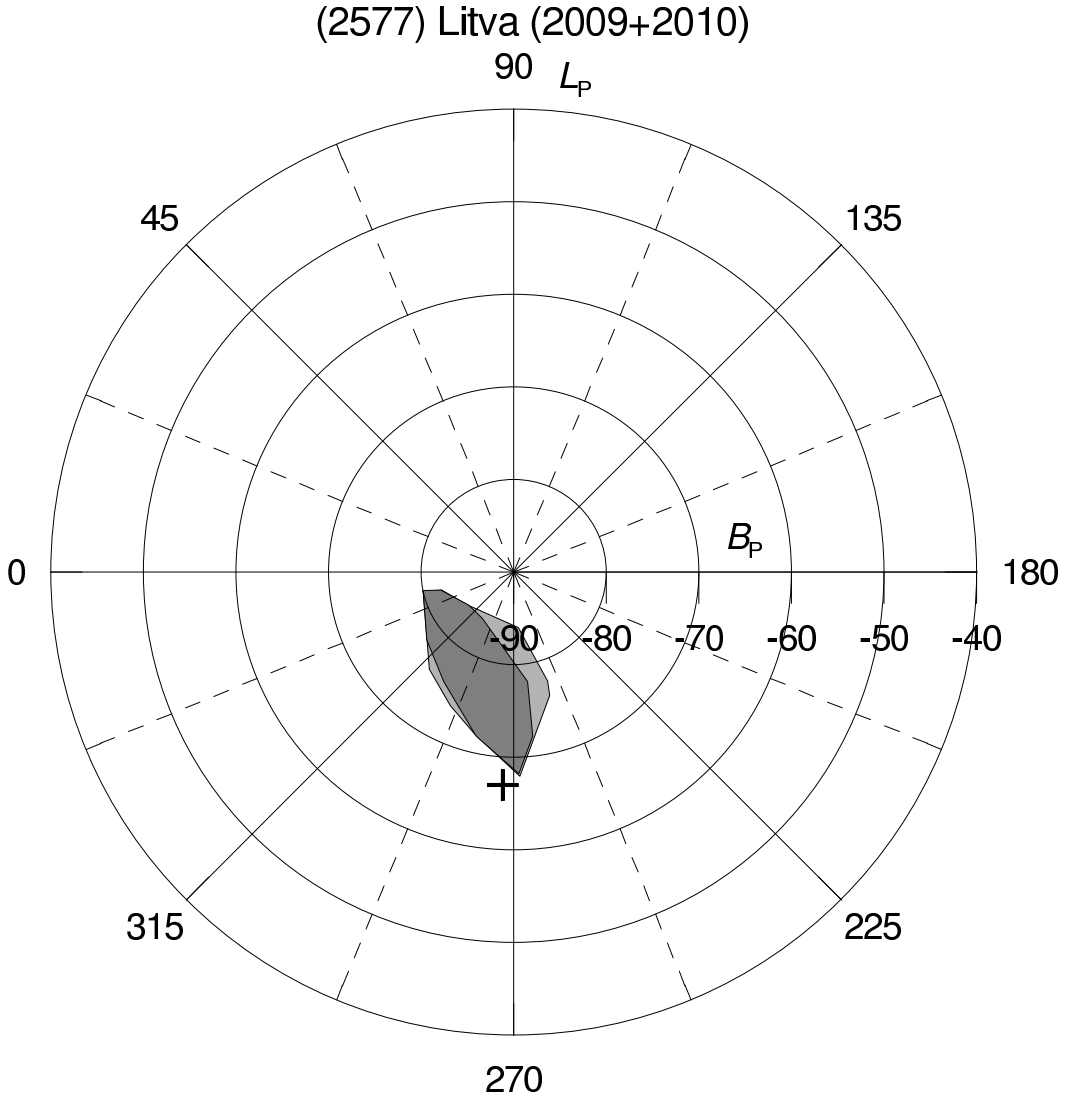

Fig. 16. Area of admissible poles for the mutual orbit of (2577) Litva in ecliptic coordinates. The solid curve inside the area bounds the admissible poles constrained using the effective diameter of the third body set equal to the effective diameter of the primary. The south pole of the current asteroid's heliocentric orbit is marked with the cross.

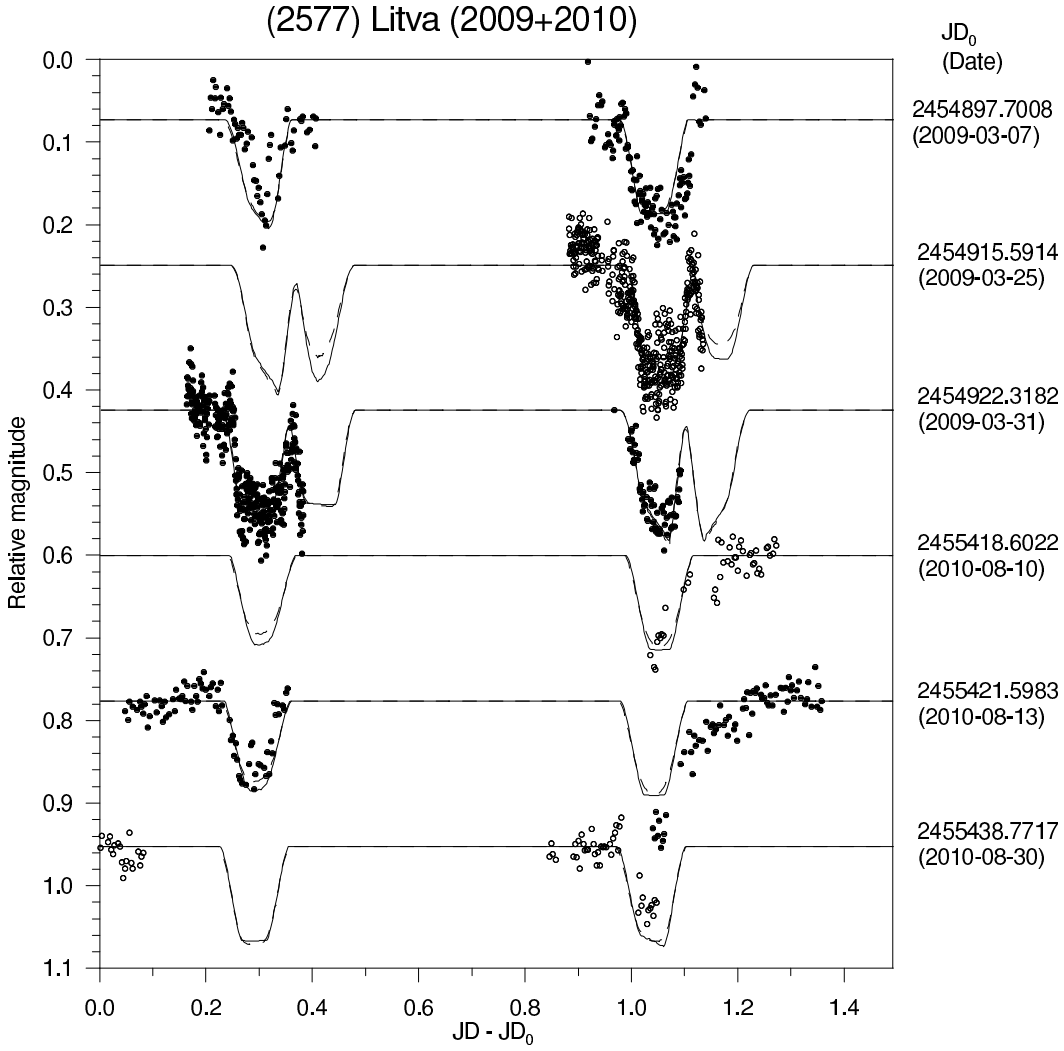

Fig. 17. Sample of the orbital lightcurve component's data of (2577) Litva in apparitions 2009 and 2010. The observational data (points) are plotted together with the synthetic lightcurve for the best-fit solution without the third body (solid curve) and with the third body with diameter equal to D_1 (dashed curve). The data sets from different dates are vertically offset for clarity, and different symbols are used for them to avoid confusion. The offsets in date (JD_0) are listed in the right column for each curve. On the third and the last curves from the top, the minima are shown in an order opposite (i.e., first the secondary and then the primary event) to the other curves.

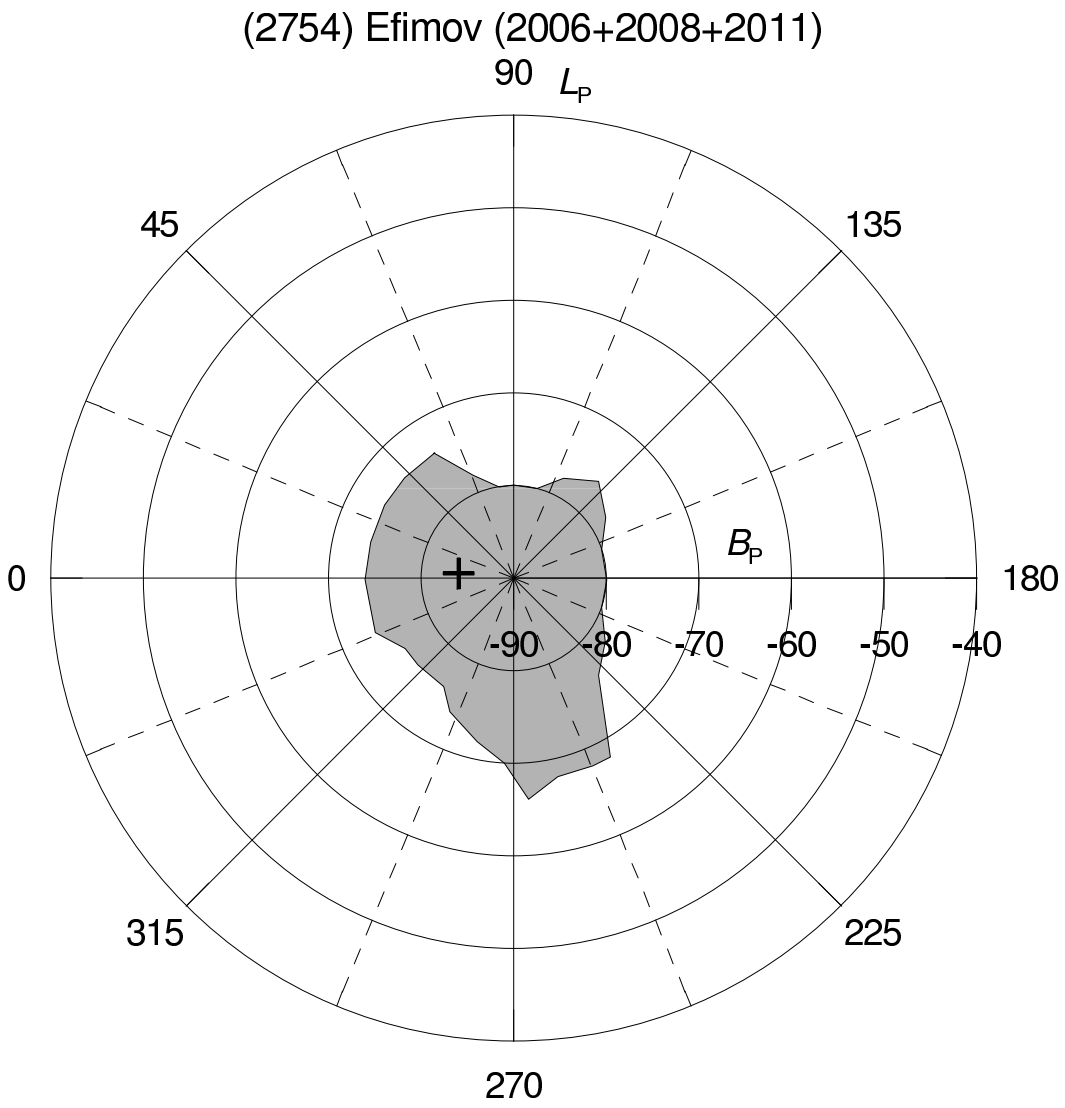

Fig. 18. Area of admissible poles for the mutual orbit of (2754) Efimov in ecliptic coordinates. The south pole of the current asteroid's heliocentric orbit is marked with the cross.

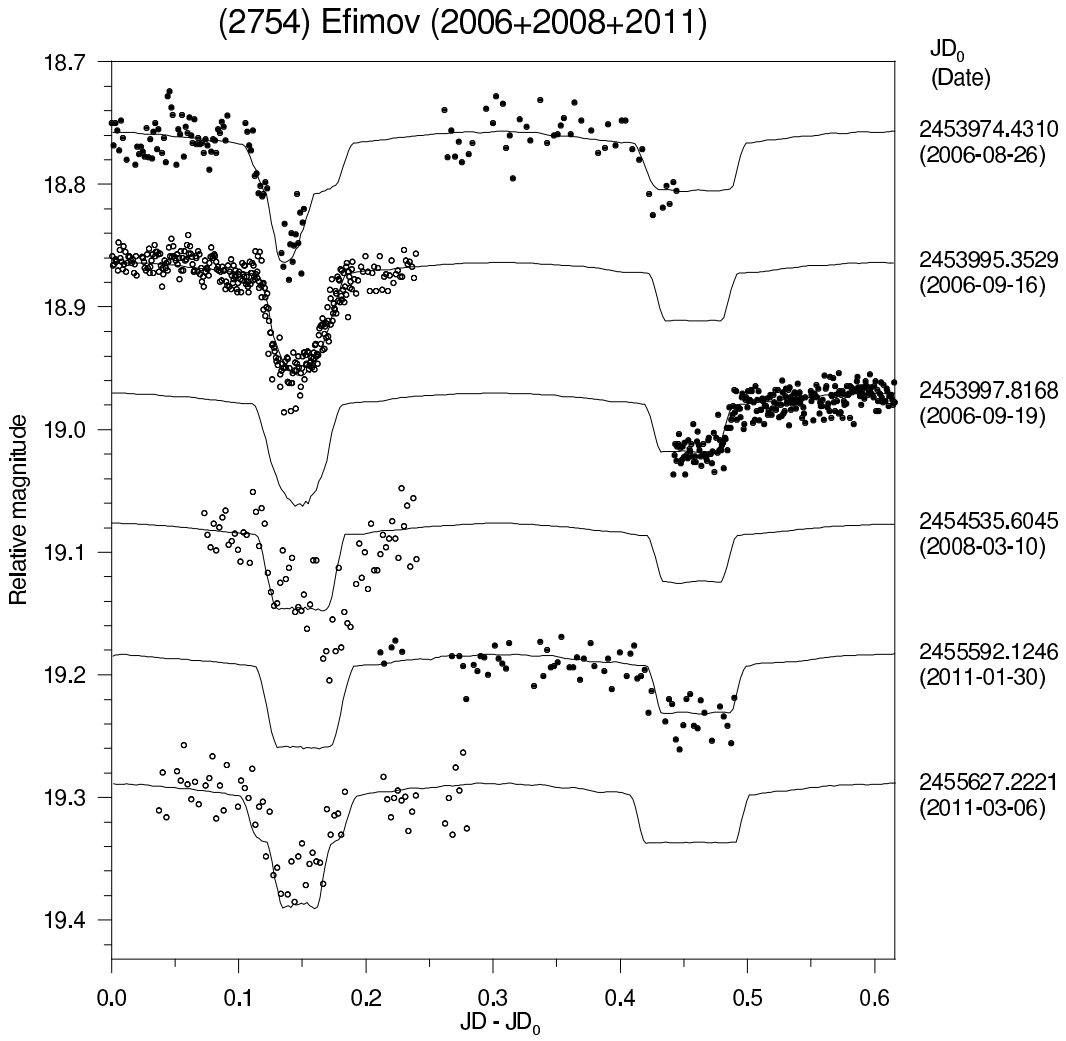

Fig. 19. Sample of the orbital lightcurve component's data of (2754) Efimov in apparitions 2006, 2008, and 2011. The observational data (points) are plotted together with the synthetic lightcurve for the best-fit solution (curve). The data sets from different dates are vertically offset for clarity, and different symbols are used for them to avoid confusion. The offsets in date (JD_0) are listed in the right column for each curve.

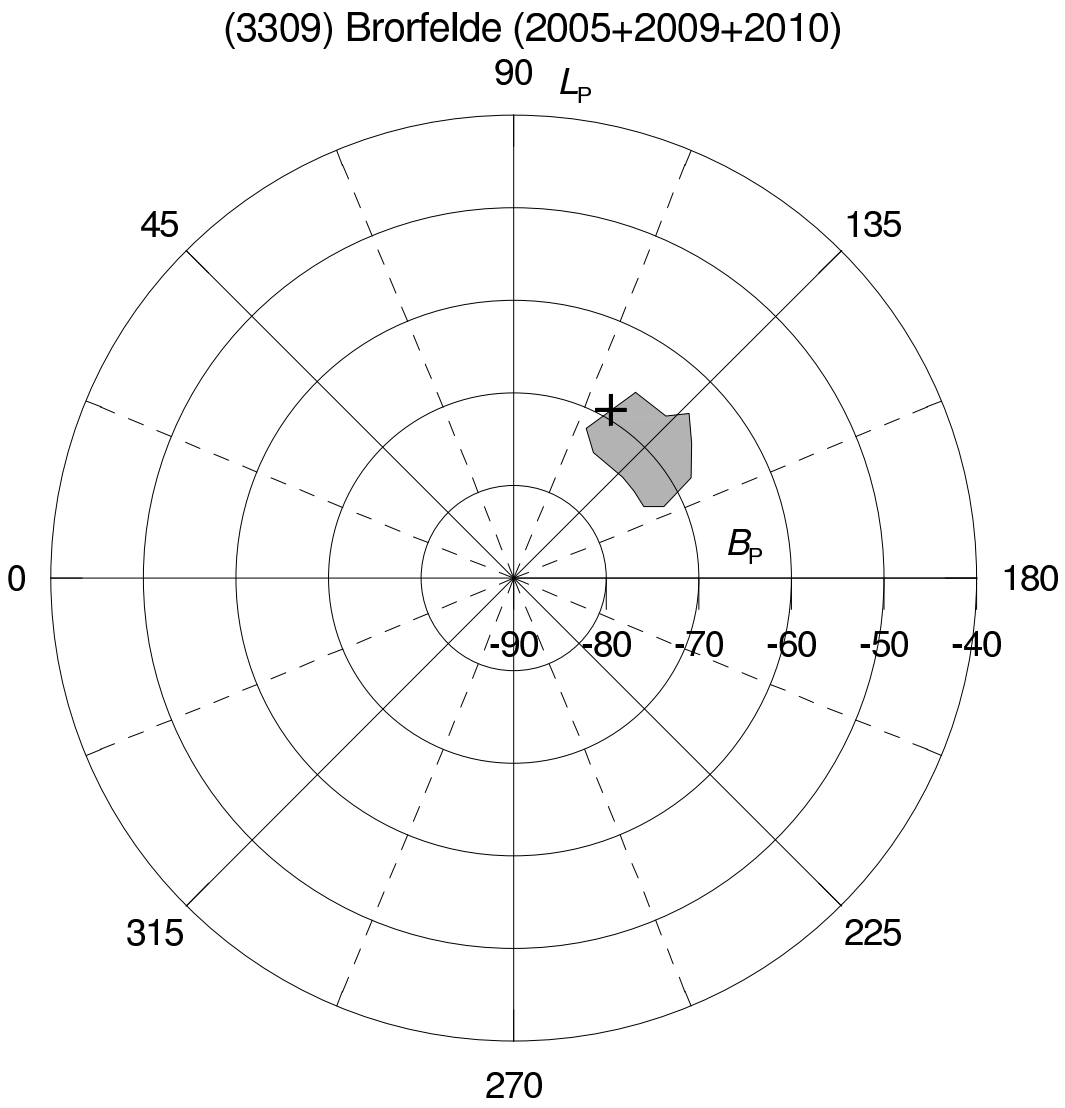

Fig. 20. Area of admissible poles for the mutual orbit of (3309) Brorfelde in ecliptic coordinates. The south pole of the current asteroid's heliocentric orbit is marked with the cross.

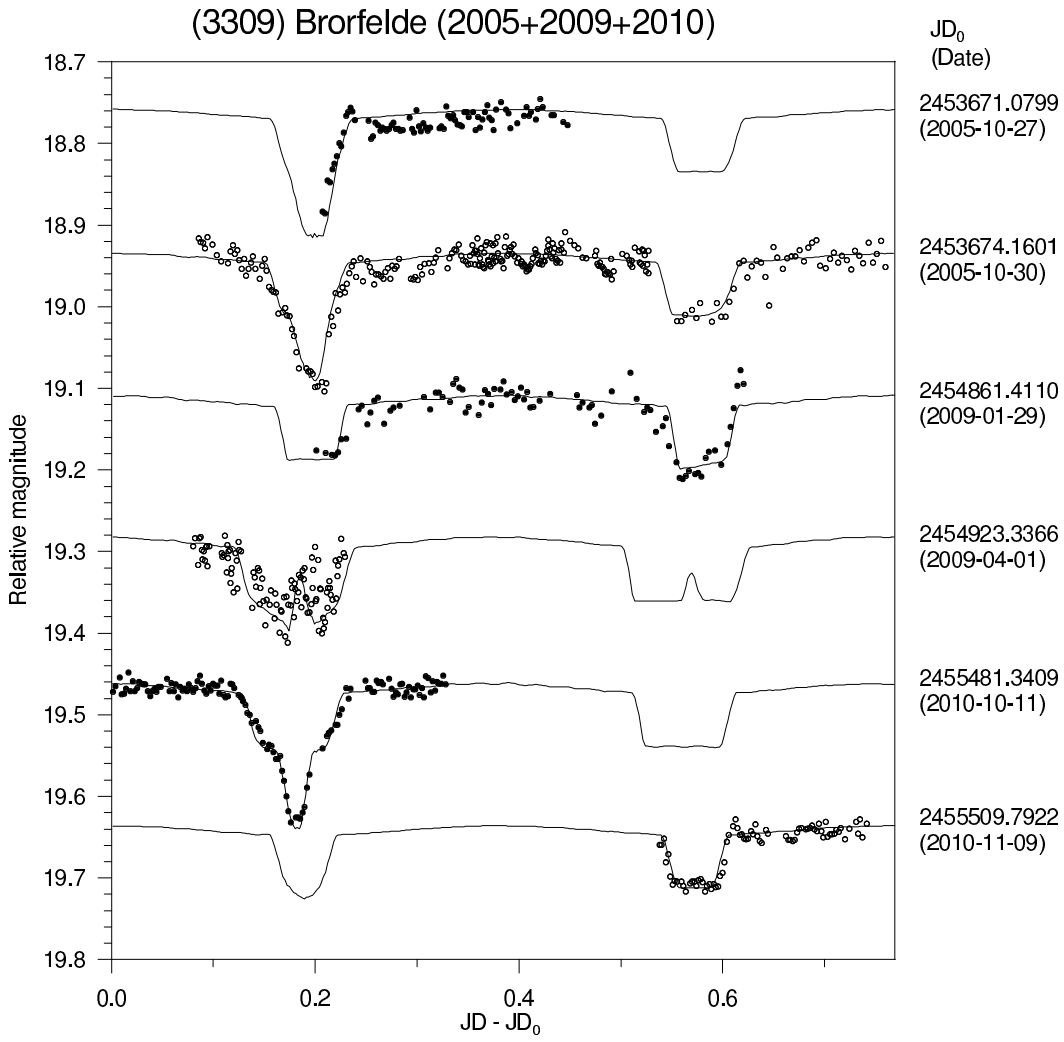

Fig. 21. Sample of the orbital lightcurve component's data of (3309) Brorfelde in apparitions 2005, 2009, and 2010. The observational data (points) are plotted together with the synthetic lightcurve for the best-fit solution (curve). The data sets from different dates are vertically offset for clarity, and different symbols are used for them to avoid confusion. The offsets in date (JD_0) are listed in the right column for each curve. On the third curve from the top, the minima are shown in an order opposite (i.e., first the secondary and then the primary event) to the other curves.

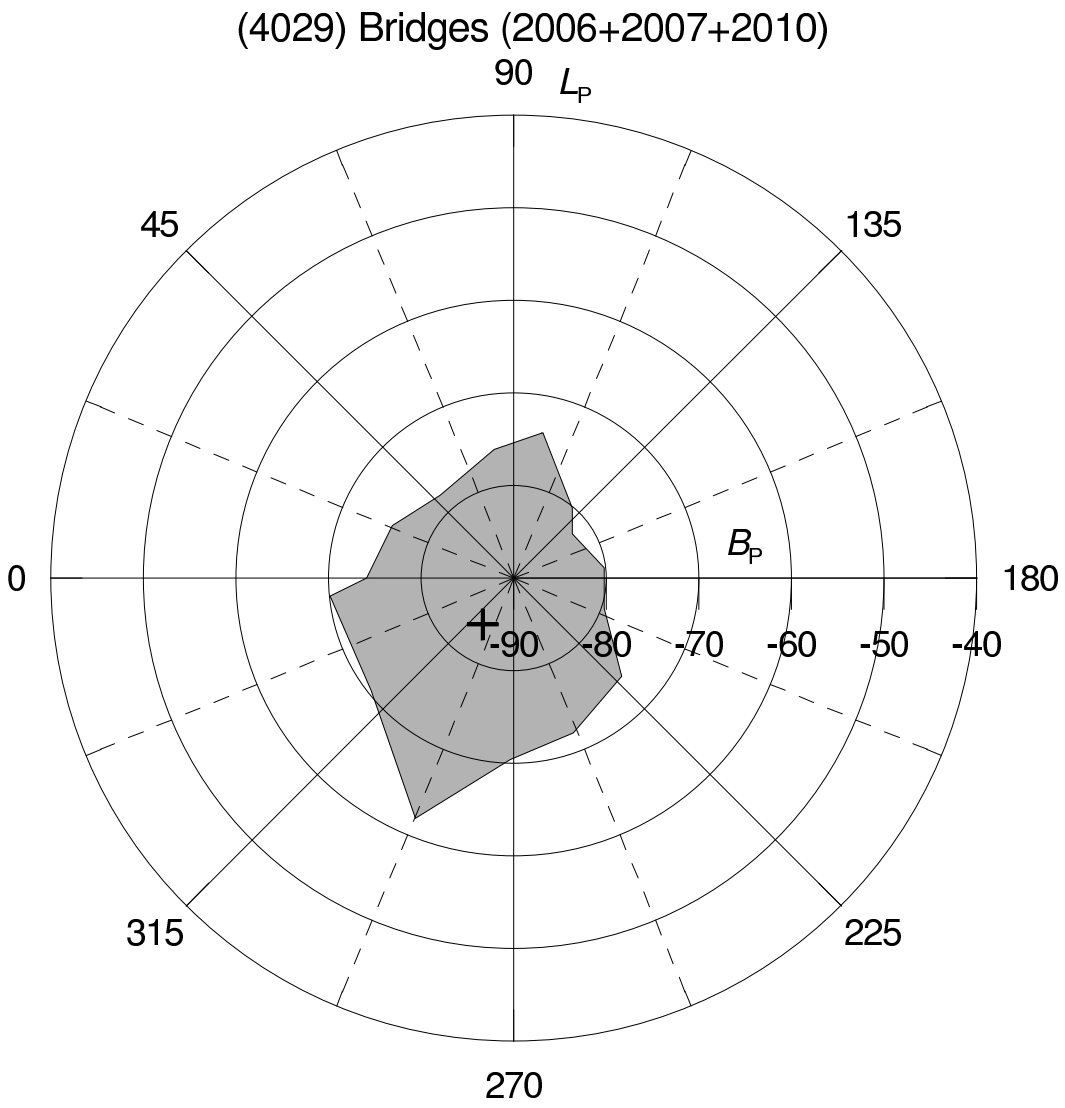

Fig. 22. Area of admissible poles for the mutual orbit of (4029) Bridges in ecliptic coordinates. The south pole of the current asteroid's heliocentric orbit is marked with the cross.

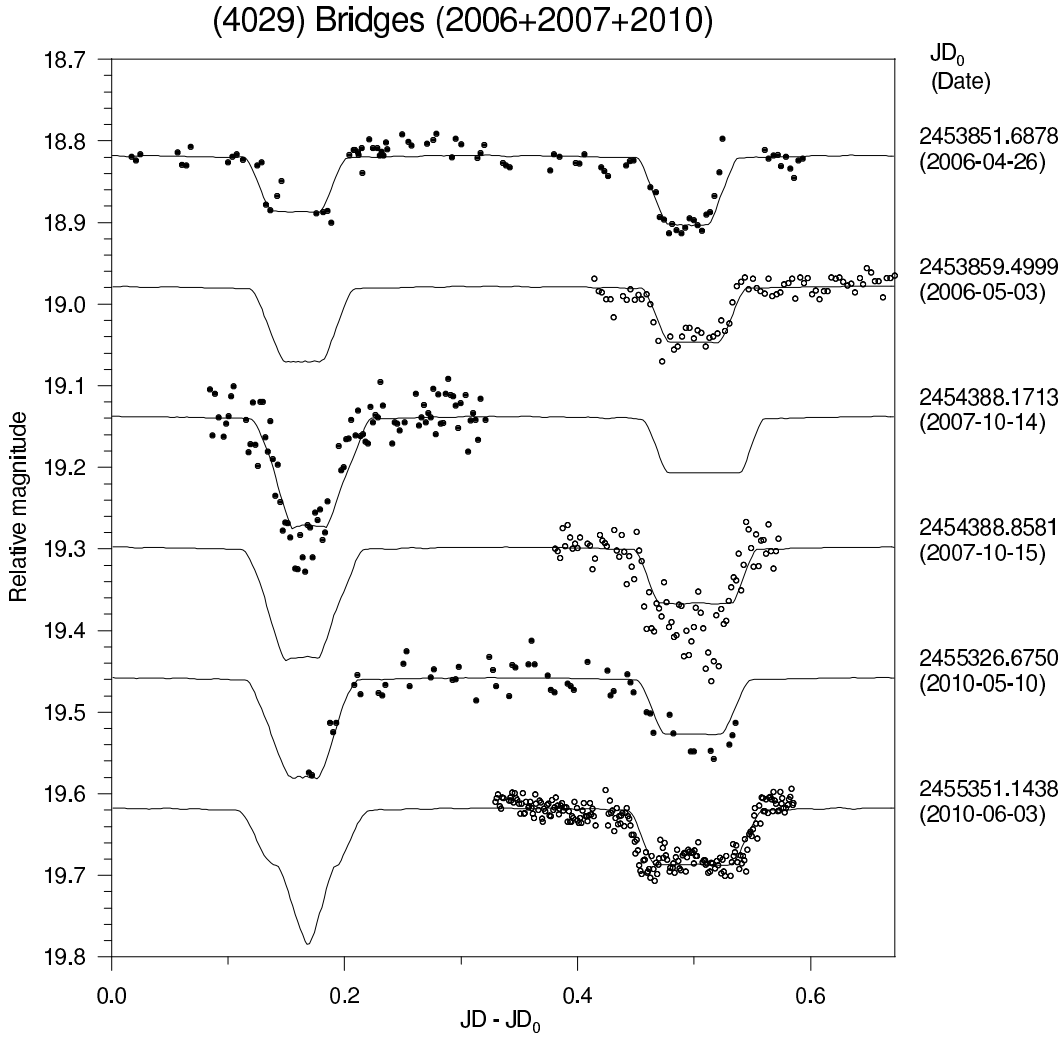

Fig. 23. Sample of the orbital lightcurve component's data of (4029) Bridges in apparitions 2006, 2007, and 2010. The observational data (points) are plotted together with the synthetic lightcurve for the best-fit solution (curve). The data sets from different dates are vertically offset for clarity, and different symbols are used for them to avoid confusion. The offsets in date (JD_0) are listed in the right column for each curve. On the first curve from the top, the minima are shown in an order opposite (i.e., first the secondary and then the primary event) to the other curves.

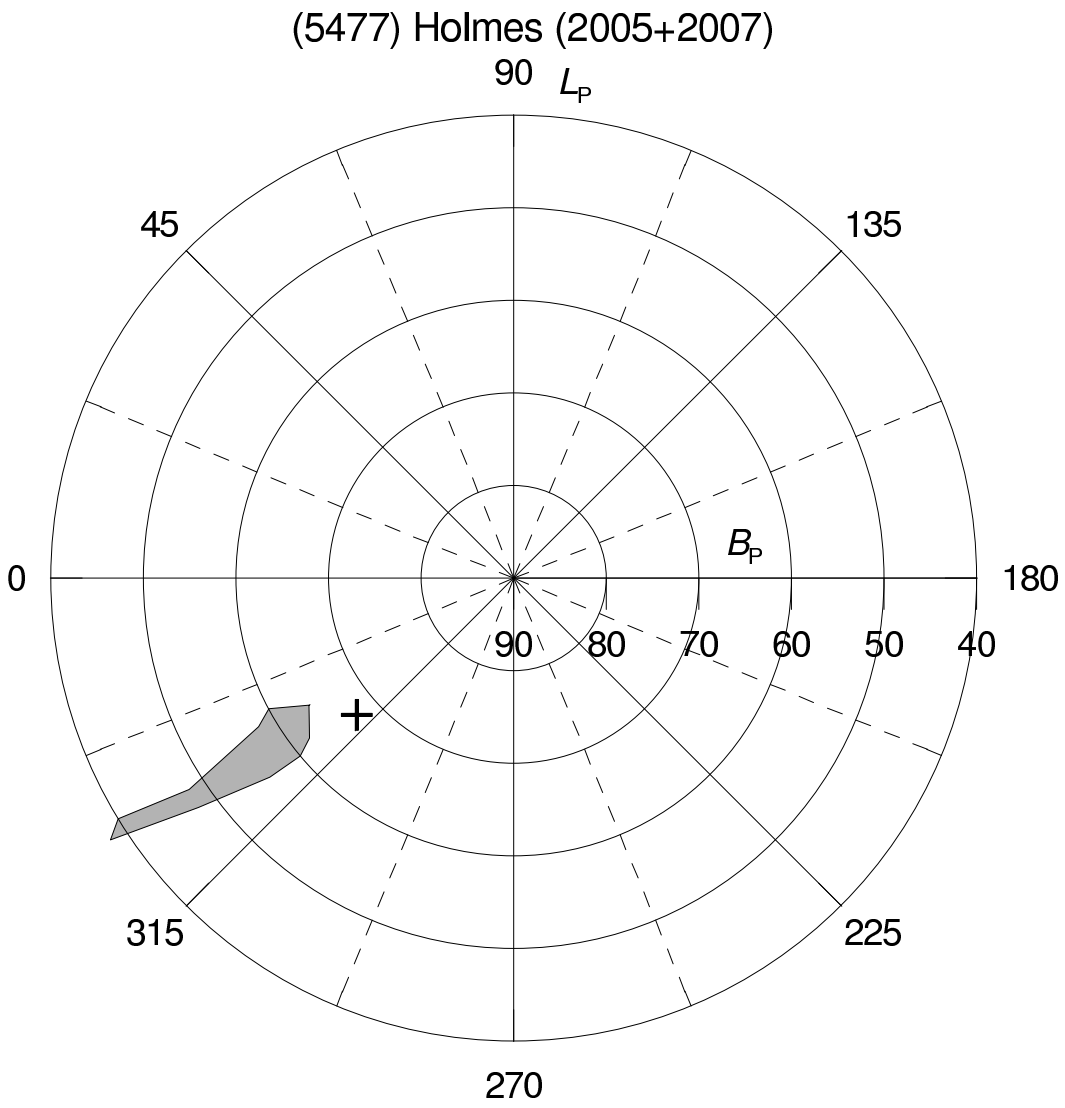

Fig. 24. Area of admissible poles for the mutual orbit of (5477) Holmes in ecliptic coordinates. The north pole of the current asteroid's heliocentric orbit is marked with the cross.

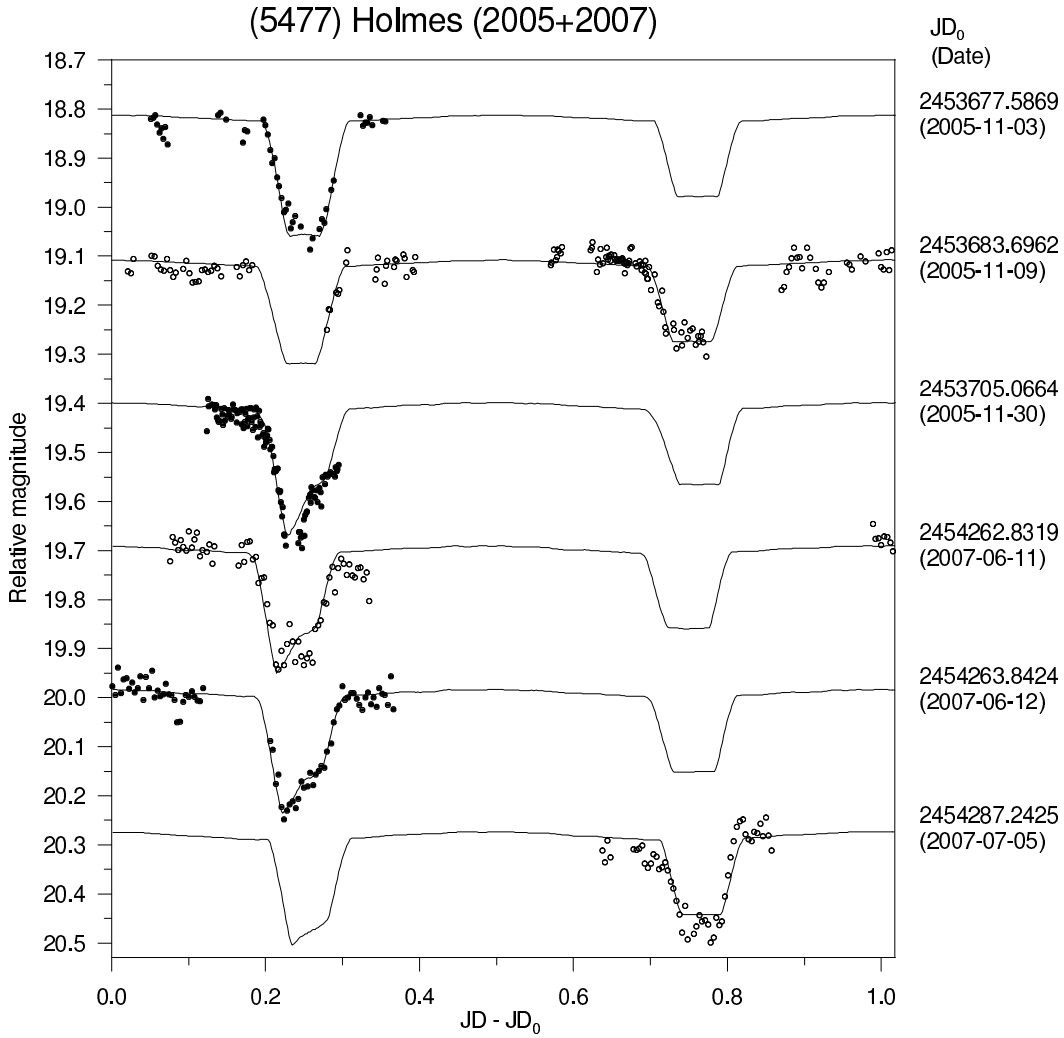

Fig. 25. Sample of the orbital lightcurve component's data of (5477) Holmes in apparitions 2005 a 2007. The observational data (points) are plotted together with the synthetic lightcurve for the best-fit solution (curve). The data sets from different dates are vertically offset for clarity, and different symbols are used for them to avoid confusion. The offsets in date (JD_0) are listed in the right column for each curve.

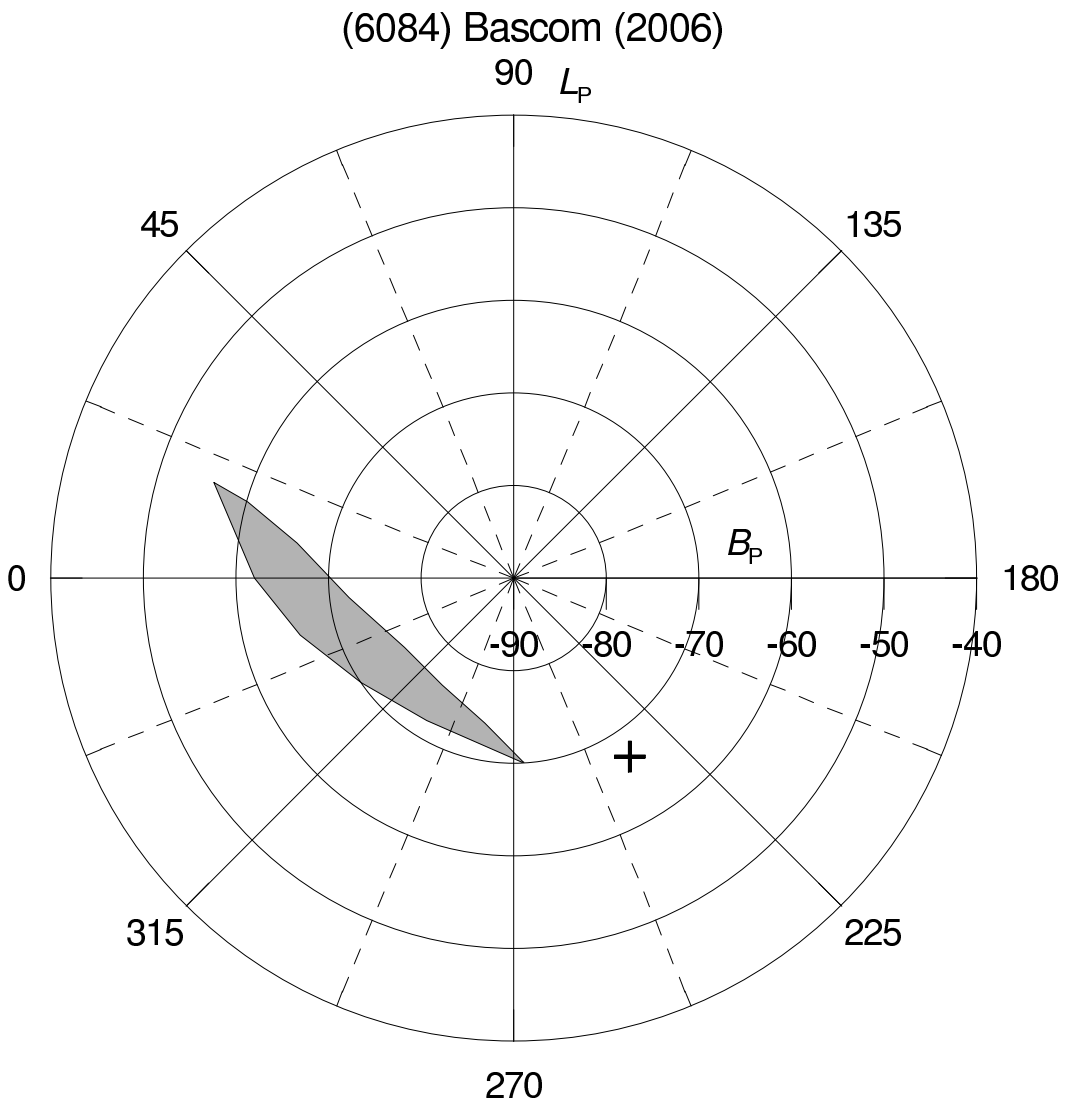

Fig. 26. Area of admissible poles for the mutual orbit of (6084) Bascom in ecliptic coordinates. The south pole of the current asteroid's heliocentric orbit is marked with the cross.

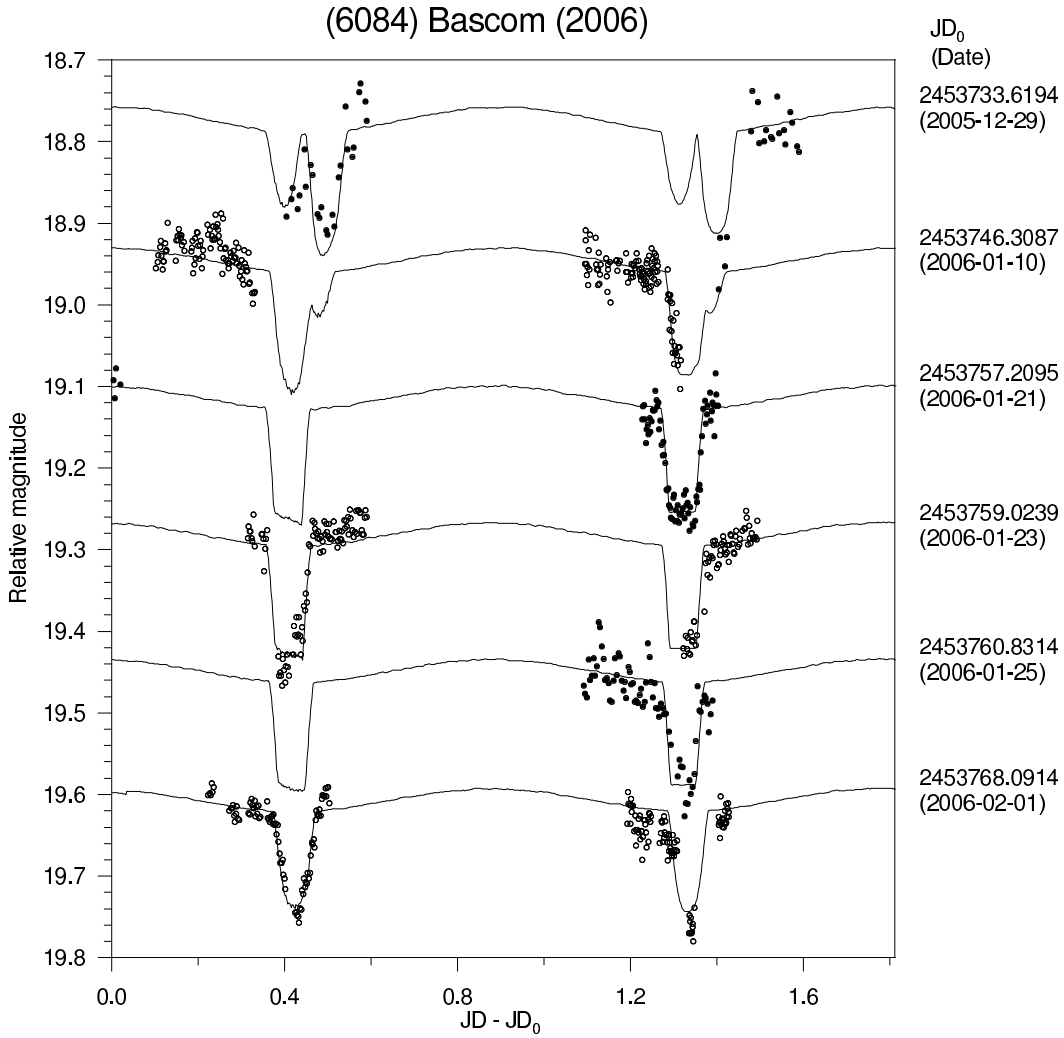

Fig. 27. Sample of the orbital lightcurve component's data of (6084) Bascom in apparition 2006. The observational data (points) are plotted together with the synthetic lightcurve for the best-fit solution (curve). The data sets from different dates are vertically offset for clarity, and different symbols are used for them to avoid confusion. The offsets in date (JD_0) are listed in the right column for each curve.

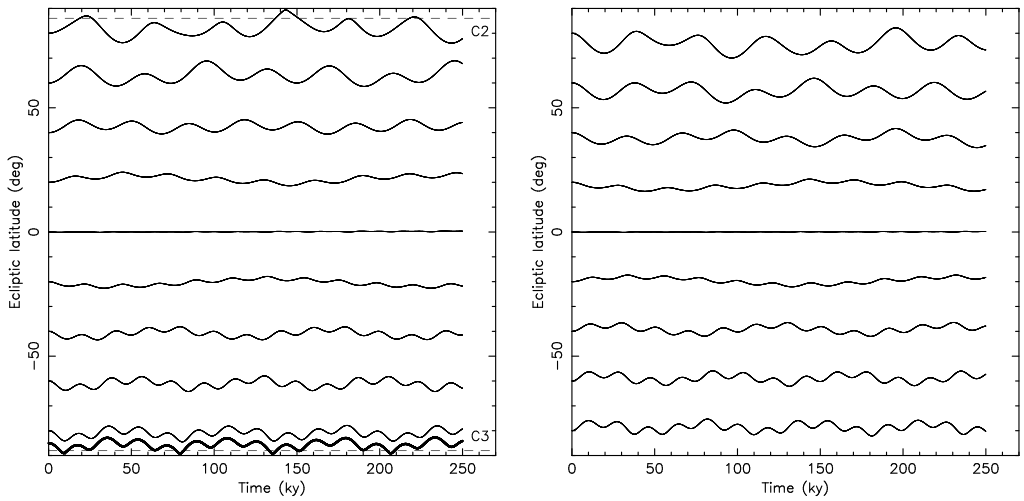

Fig. 28. A sample of evolutionary tracks of the ecliptic latitude (ordinate) of the orbital pole for (4029) Bridges determined by our numerical model; the abscissa is time in ky. Initial ecliptic latitudes $B_{\rm p}$ were $0°$, $\pm 20°$, $\pm 40°$, $\pm 60°$ and $\pm 80°$. Results on the left panel had initial orbit pole with ecliptic longitude $L_{\rm p,1} = \Omega + 90°$, while those on the right panel had $L_{\rm p,2} = \Omega + 270°$, where Ω is the longitude of ascending node of the binary's heliocentric orbit (cf. Appendix). The gray dashed lines on the left panel show ecliptic latitudes of the Cassini states 2 and 3. The thick curve on the left panel shows a possible evolution of Bridges' pole with initial data $(L_{\rm p}, B_{\rm p}) = (305°, -85°)$ very close to the osculating pole of the heliocentric orbit and near the center of the uncertainty region of the solution (Table 1 and Fig. 22). All orbits are stable, independently of the latitude value, with only small oscillations due to small value of the heliocentric orbit inclination to the ecliptic.

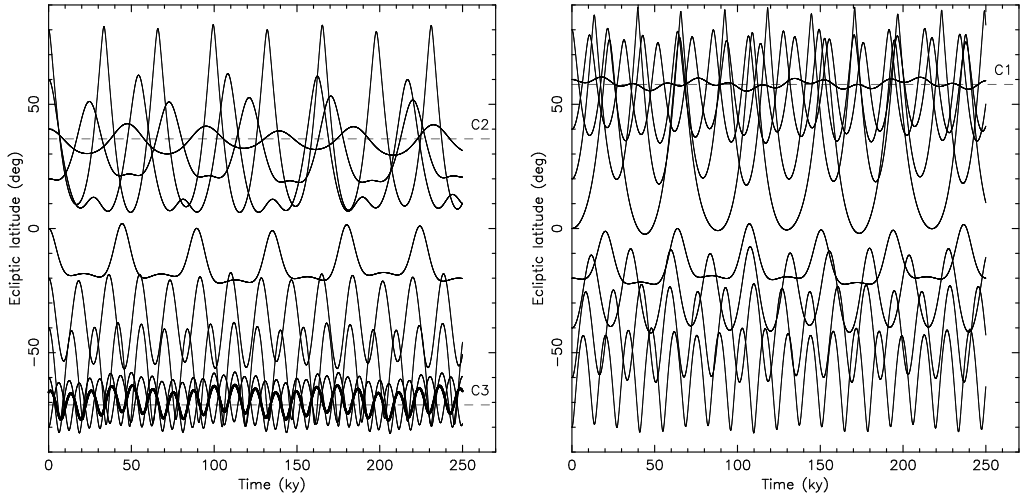

Fig. 29. The same as in Fig. 28, but for the Hungaria-class binary (1453) Fennia. The gray dashed lines now show ecliptic latitude of the Cassini states 1, 2 and 3. The thick curve shows a possible evolution of the orbit pole for this binary for initial position $(L_\mathrm{p}, B_\mathrm{p}) = (95^\circ, -66^\circ)$ very close to the osculating pole of the heliocentric orbit and near the center of the uncertainty region of the solution (Table 1 and Fig. 10).

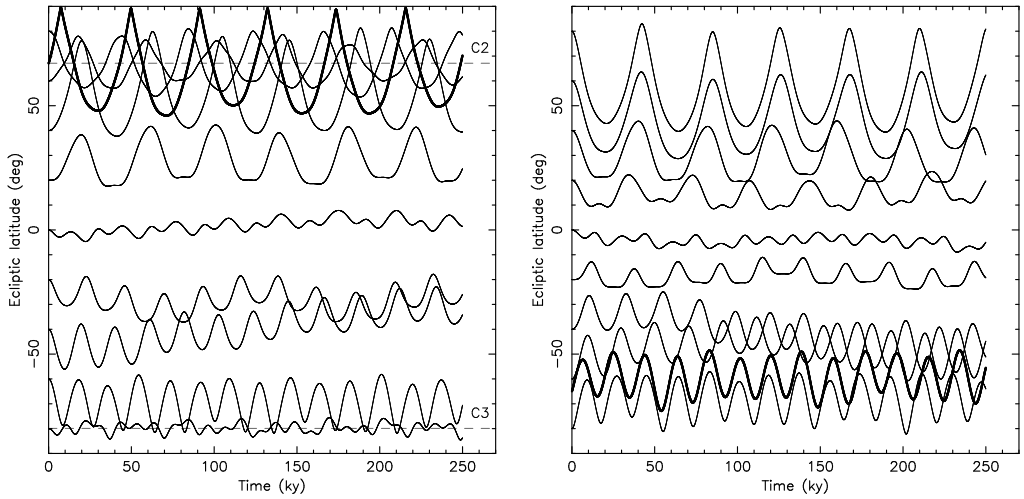

Fig. 30. The same as in Fig. 28, but for the Phocaea-class binary (2044) Wirt. The gray dashed lines now show ecliptic latitude of the Cassini states 1, 2 and 3. The thick curves show a possible evolution of the two solutions of the orbit pole for this binary (see Table 1 and Fig. 14): initial pole position $(L_\mathrm{p}, B_\mathrm{p}) = (180^\circ, 67^\circ)$ on the left panel and $(L_\mathrm{p}, B_\mathrm{p}) = (0^\circ, -65^\circ)$ on the right panel.